Supplemental Data

FOXA2-mediated GDF15 secretion drives metastasis and CD8$^+$ T cell exhaustion in clear cell renal cell carcinoma

Cong Huang, Rui Rui, Heng Guo, Anbang He, Wenzhi Gao, Jian Fan, Cuijian Zhang, Yanqing Gong, Liqun Zhou, Xuesong Li, Shiming He

Supplemental Figures 1–17, **Supplemental Methods**, and **Supplemental Tables 1–3**

Supplemental Figures

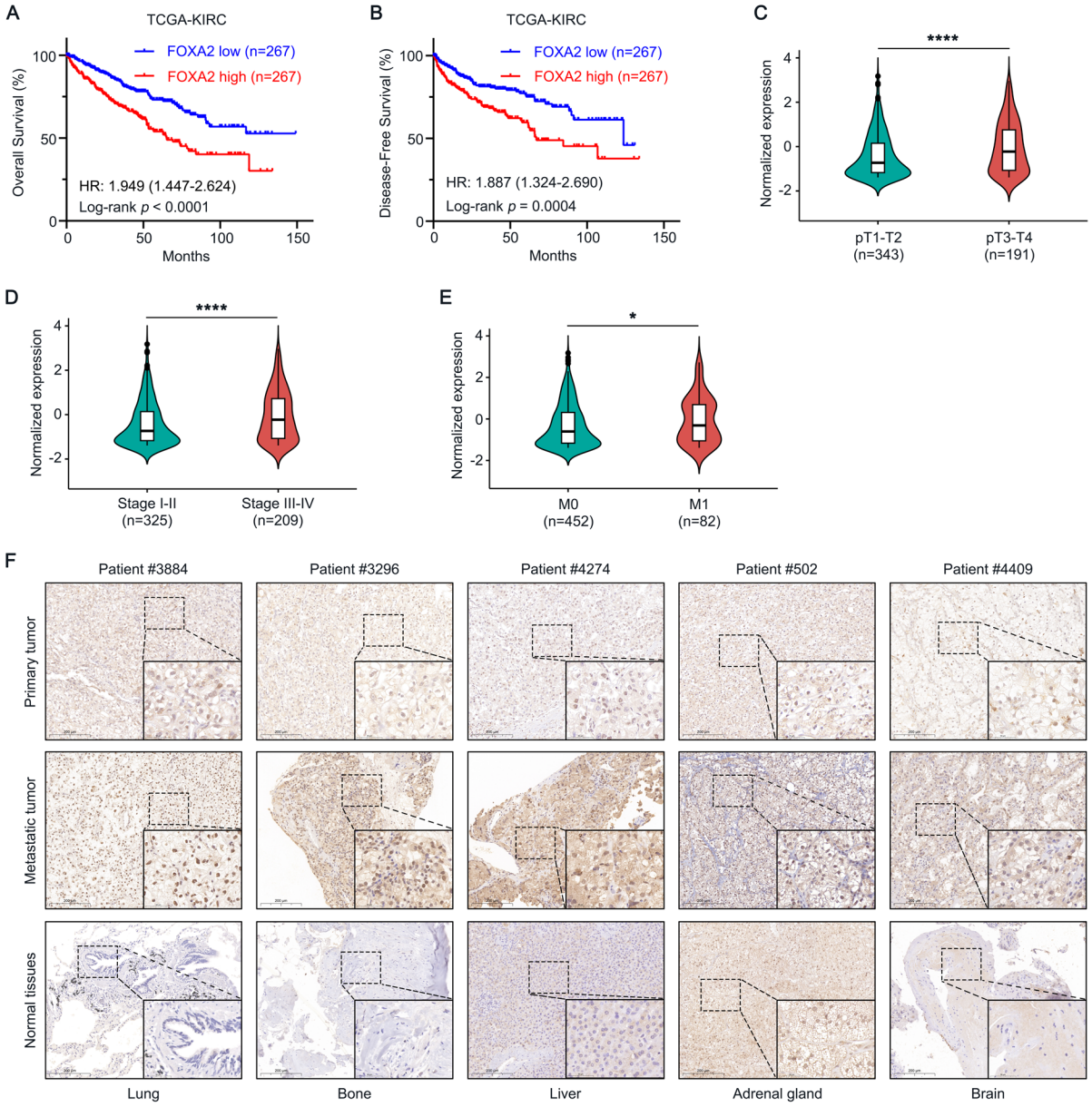


Figure S1. Elevated FOXA2 expression in TCGA-KIRC and metastatic ccRCC tissues.

(**A** and **B**) Kaplan-Meier analyses for overall survival (A) and disease-free survival (B) in patients with high versus low FOXA2 mRNA expression based on The Cancer Genome Atlas Kidney Renal Clear Cell Carcinoma (TCGA-KIRC) datasets.

(**C-E**) Violin plots of comparing FOXA2 mRNA expression between patients stratified with pathological T stage (pT1-T2 *vs.* pT3-T4; C), clinical stage (stage I-II *vs.* stage II-IV; D), and metastatic status (M0 *vs.* M1; E).

(**F**) Representative immunohistochemistry (IHC) staining of FOXA2 expression in paired primary and metastatic clear cell renal cell carcinoma (ccRCC) tissues. Scale bars, 200 μm.

Data are presented as mean ± SD. *p* values were obtained by log-rank test (A and B), and two-tailed, unpaired Student's *t*-tests (C-E). $^{*}p < 0.05$, $^{****}p < 0.0001$.

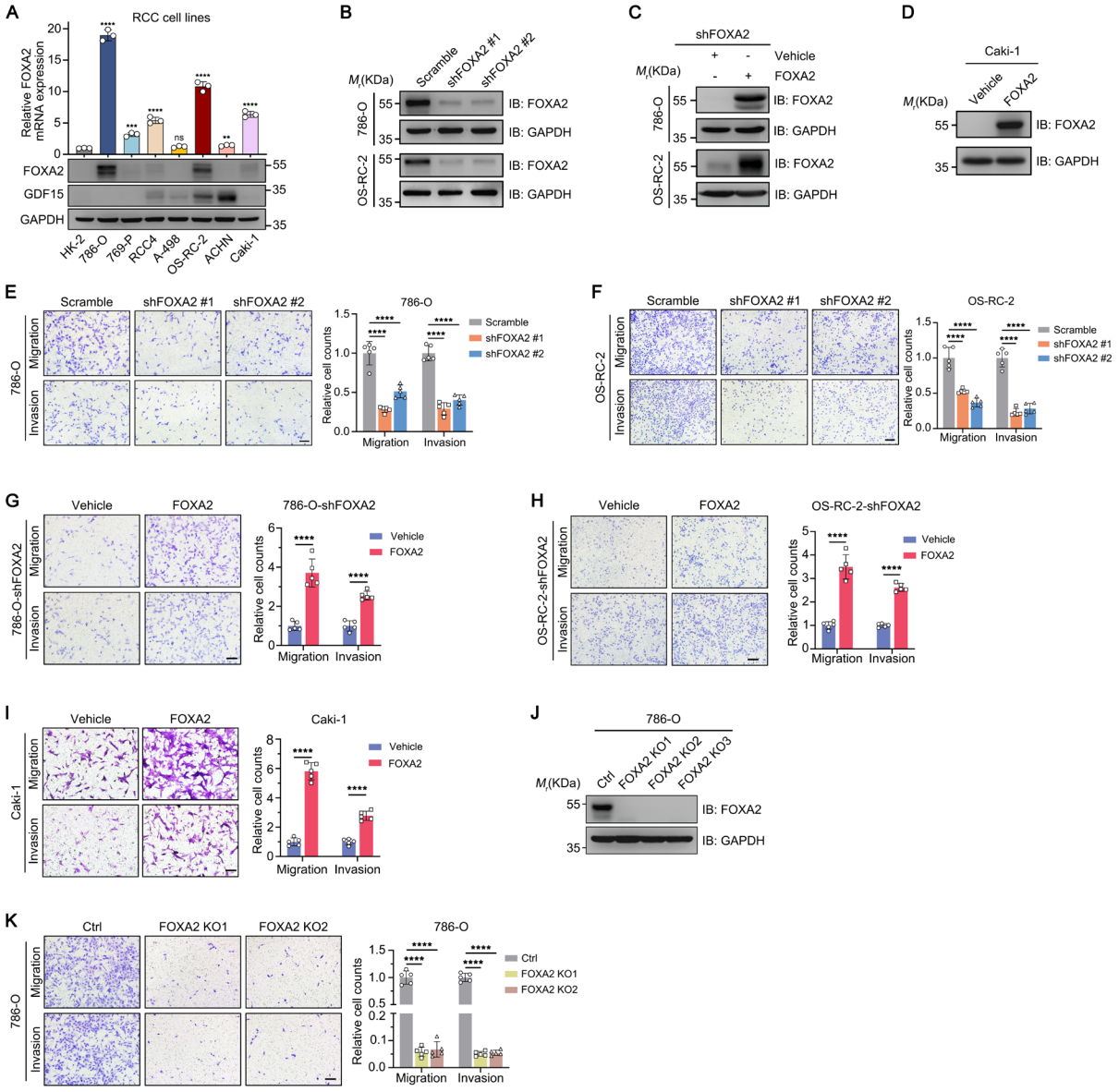


Figure S2. FOXA2 promotes ccRCC metastasis *in vitro*.

(**A**) RT-qPCR and western blotting analysis of FOXA2 and GDF15 expression in HK-2 and various RCC cell lines.

(**B**) Western blotting analysis for the efficiency of FOXA2 knockdown in 786-O and OS-RC-2 cells.

(**C**) Western blotting analysis for the efficiency of FOXA2 overexpression in 786-O and OS-RC-2 cells stably transfected with FOXA2 shRNA.

(**D**) Western blotting analysis for the efficiency of FOXA2 overexpression in Caki-1 cells.

(**E**) Representative images (left) and quantification (right) of transwell migration and invasion assays in scramble or FOXA2 knockdown 786-O cells. Scale bar, 100 μm.

(**F**) Representative images (left) and quantification (right) of transwell migration and invasion assays in scramble or FOXA2 knockdown OS-RC-2 cells. Scale bar, 100 μm.

(**G-I**) Representative images (left) and quantification (right) of transwell migration and invasion assays in vehicle or FOXA2 overexpression 786-O (G), OS-RC-2 (H), and Caki-1 (I) cells. Scale bar, 100 μm.

(**J**) Western blotting analysis for the efficiency of FOXA2 deletion using CRISPR-Cas9 in 786-O cells.

(**K**) Representative images (left) and quantification (right) of transwell migration and invasion assays in control or FOXA2 knockout 786-O cells. Scale bar, 100 μm.

Data are presented as mean ± SD. *p* values were obtained by one-way ANOVA followed by Dunnett's multiple-comparison test (E, F, and K) and two-tailed, unpaired Student's *t*-tests (A and G-I). $^{**}p < 0.01$, $^{***}p < 0.001$, $^{****}p < 0.0001$. ns, not significant.

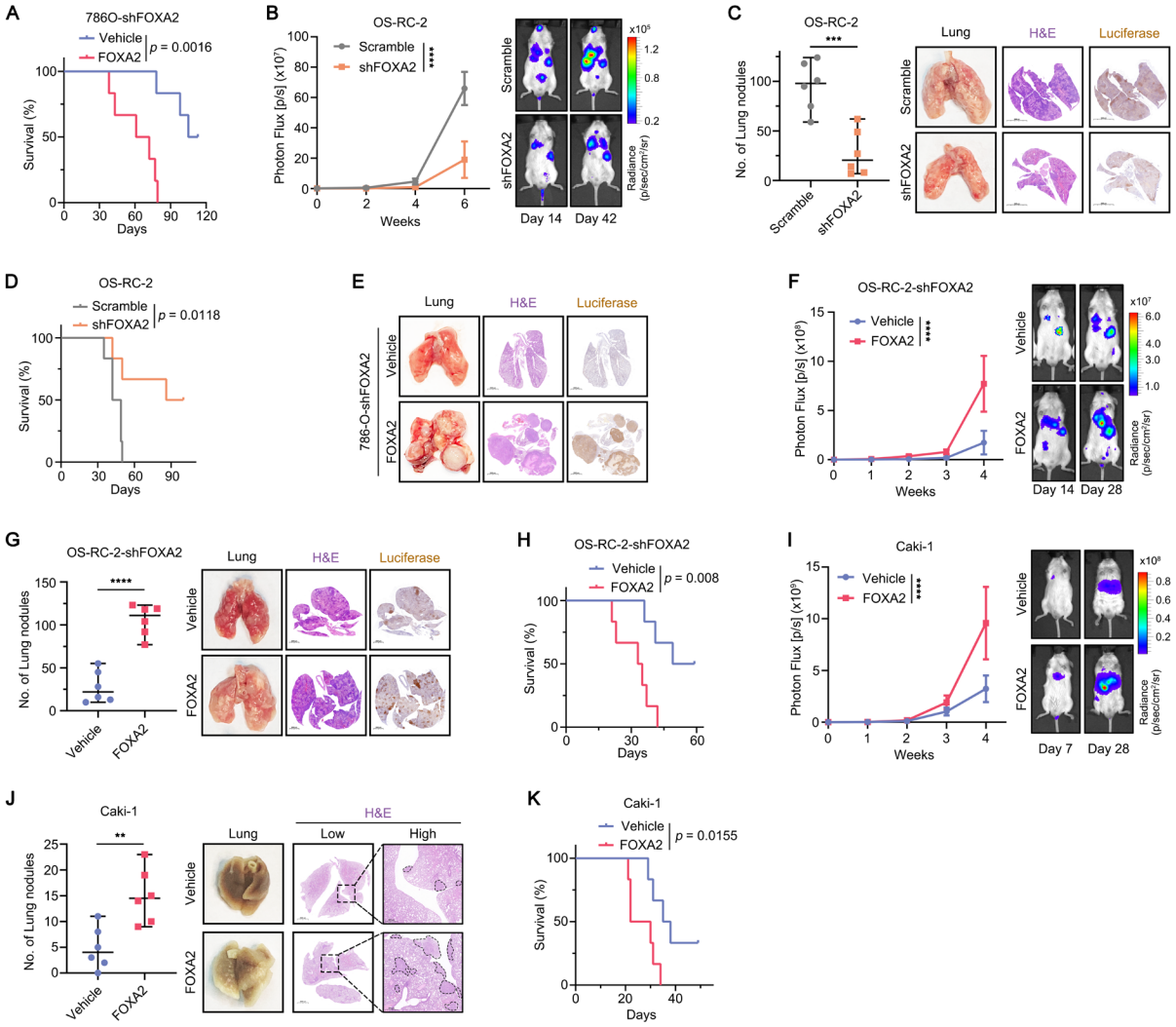


Figure S3. FOXA2 promotes ccRCC lung metastasis *in vivo*.

(**A**) Survival analysis of B-NDG mice after intravenous injection of vehicle or FOXA2 restoration 786-O cells. (n = 6 mice per group).

(**B-D**) Intravenous injection of OS-RC-2 with FOXA2 knockdown for lung metastasis analysis. Shown are bioluminescence imaging (BLI) analyses (B), lung metastatic nodules (C), and survival analysis (D) of the B-DNG mice (n = 6 mice per group). Scale bar, 2000 μm.

(**E**) Representative images of dissected lungs, hematoxylin and eosin (H&E), and luciferase IHC staining after intravenous injection of vehicle or FOXA2 restoration 786-O cells. Scale bar, 2000 μm.

(**F-H**) Intravenous injection of OS-RC-2 with FOXA2 restoration for lung metastasis analysis. Shown are BLI analyses (F), lung metastatic nodules (G), and survival analysis (H) of the B-DNG mice (n = 6 mice per group). Scale bar, 2000 μm.

(**I-K**) Intravenous injection of Caki-1 with FOXA2 overexpression for lung metastasis analysis. Shown are BLI analyses (I), lung metastatic nodules (J), and survival analysis (K) of the B-DNG mice (n = 6 mice per group). Scale bar, 2000 μm.

Data are presented as mean ± SD. *p* values were calculated using log-rank test (A, D, H, and K), two-tailed, unpaired Student's *t*-tests (C, G, and J), and two-way ANOVA (B, F, and I). $^{**}p < 0.01$. $^{***}p < 0.001$. $^{****}p < 0.0001$.

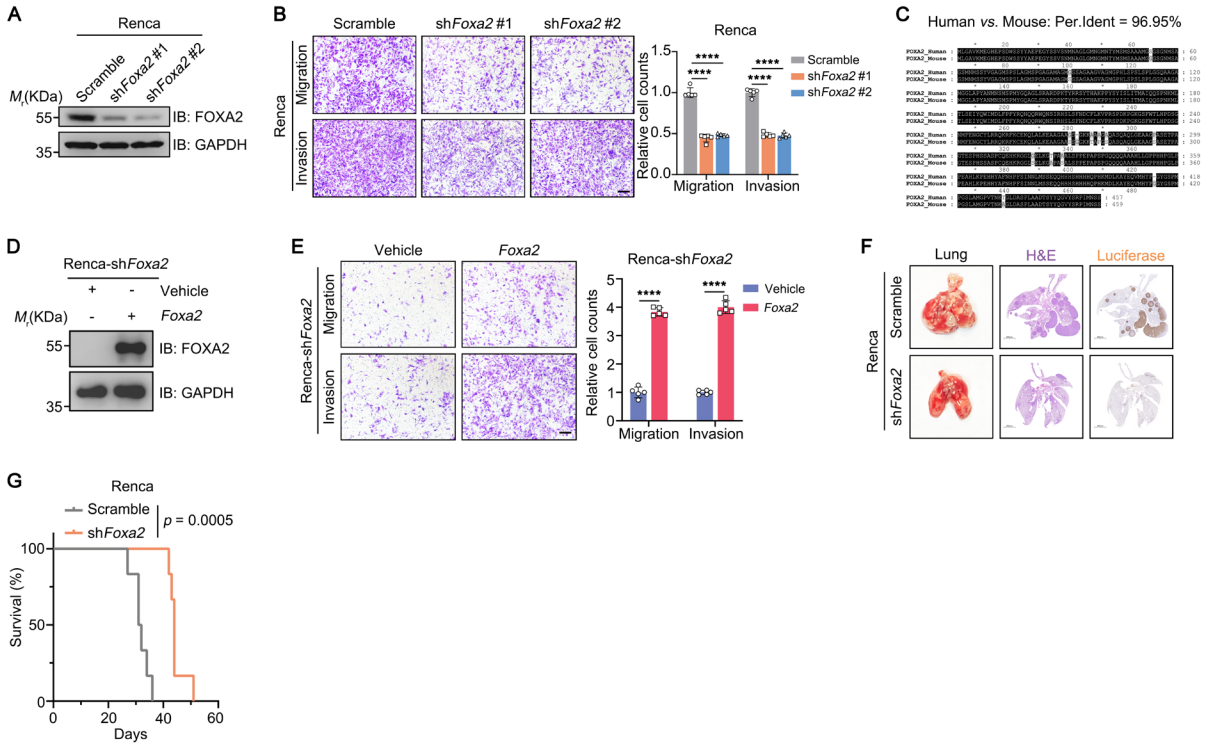


Figure S4. *Foxa2* promotes Renca cell metastasis.

(**A**) Western blotting analysis for the efficiency of *Foxa2* knockdown in Renca cells.

(**B**) Representative images (left) and quantification (right) of transwell migration and invasion assays in scramble or *Foxa2* knockdown Renca cells. Scale bar, 100 μm.

(**C**) Protein sequence alignment showing percentage identity between human FOXA2 and murine *Foxa2*.

(**D**) Western blotting analysis for the efficiency of *Foxa2* overexpression in Renca cells.

(**E**) Representative images (left) and quantification (right) of transwell migration and invasion assays in vehicle or *Foxa2* overexpression Renca cells. Scale bar, 100 μm.

(**F**) Representative images of dissected lungs, H&E, and luciferase IHC staining after intravenous injection of scramble or *Foxa2* knockdown Renca cells. Scale bar, 2000 μm.

(**G**) Survival analysis of BALB/c mice after intravenous injection of scramble and *Foxa2* knockdown Renca cells (n = 6 mice per group).

Data are presented as mean ± SD. *p* values were calculated using one-way ANOVA followed by Dunnett's multiple-comparison test (B), two-tailed, unpaired Student's *t*-tests (E), and log-rank test (G). $^{****}p < 0.0001$.

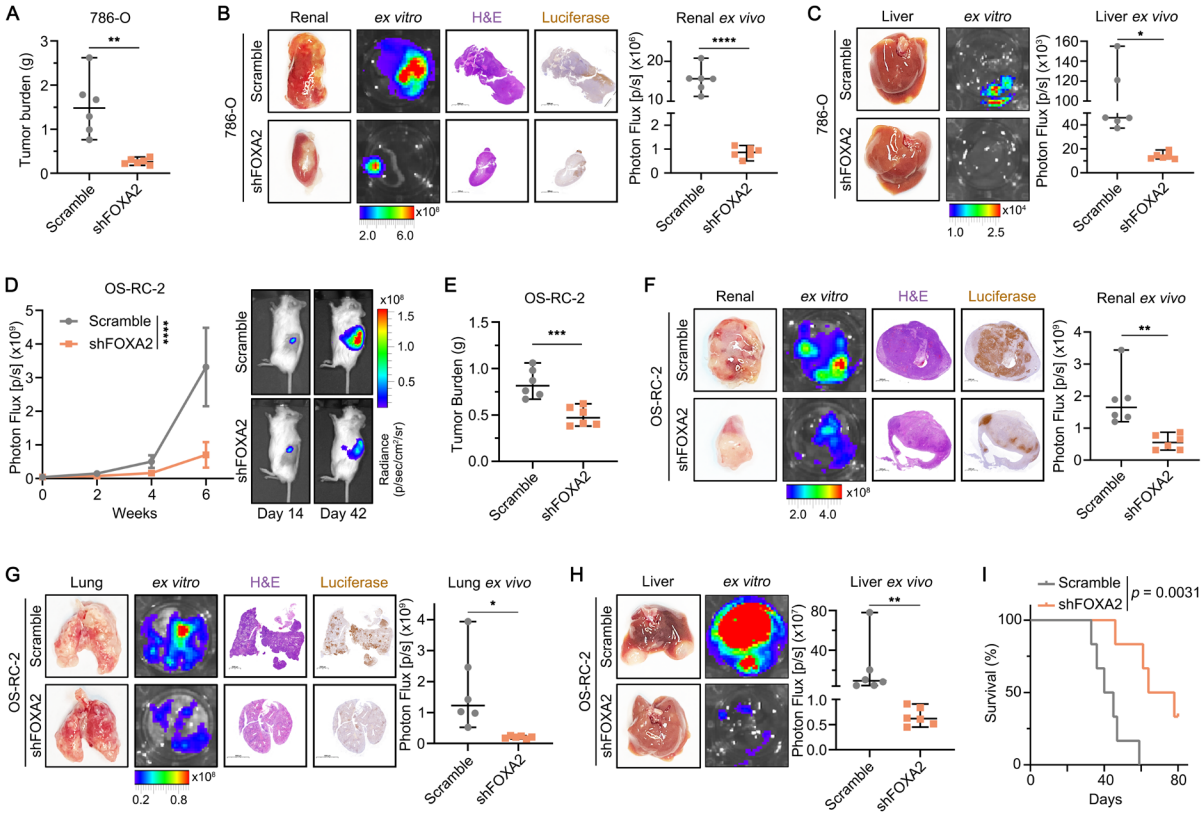


Figure S5. FOXA2 knockdown inhibits spontaneous metastasis of ccRCC *in vivo*.

(**A**) Quantification of tumor burden in B-NDG mice orthotopically implanted with scramble or FOXA2 knockdown 786-O cells (n = 6 mice per group).

(**B**) Representative images of dissected renal, *ex vivo* bioluminescence, H&E, and luciferase IHC staining (left), and quantification of renal photon flux (right) following orthotopic implantation of scramble or FOXA2 knockdown 786-O cells (n = 6 mice per group). Scale bar, 2000 µm.

(**C**) Representative images of dissected liver and *ex vivo* bioluminescence (left), and quantification of liver photon flux (right) following orthotopic implantation of scramble or FOXA2 knockdown 786-O cells (n = 6 mice per group). Scale bar, 2000 µm.

(**D-I**) Orthotopic implantation of OS-RC-2 cells with FOXA2 knockdown for spontaneous metastasis analysis. Shown are BLI analyses (D), orthotopic tumor burden (E and F), lung metastases (G), liver metastases (H), and survival analysis (I) in B-DNG mice (n = 6 mice per group). Scale bar, 2000 µm.

Data are presented as mean ± SD. *p* values were determined with two-tailed, unpaired Student's *t*-tests (A-C, and E-H), two-way ANOVA (D), and log-rank test (I). $^{*}p < 0.05$. $^{**}p < 0.01$. $^{***}p < 0.001$. $^{****}p < 0.0001$.

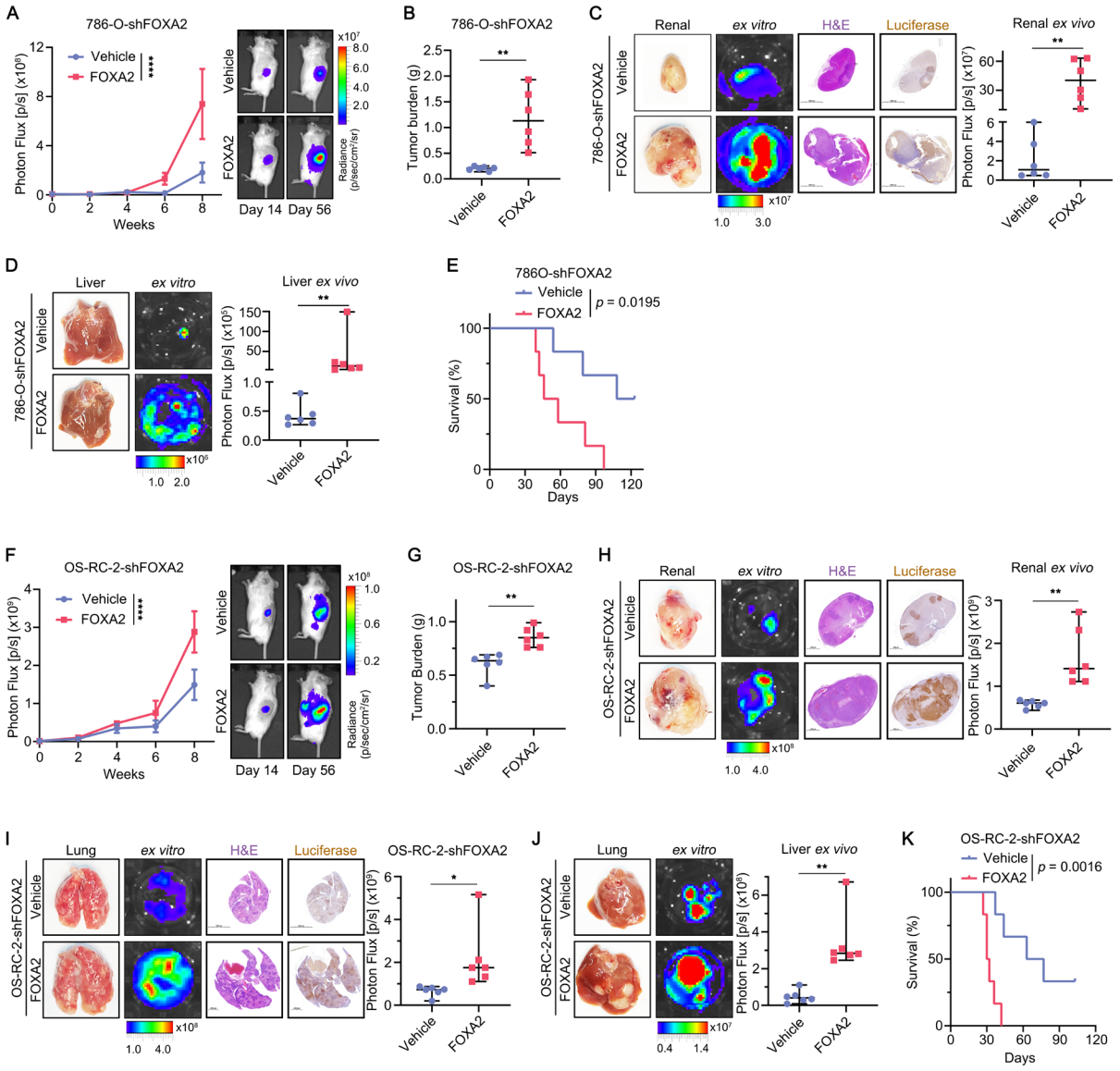


Figure S6. FOXA2 overexpression facilitates spontaneous metastasis of ccRCC *in vivo*.

(**A-E**) Orthotopic implantation of 786-O cells with FOXA2 restoration for spontaneous lung metastasis analysis. Shown are BLI analyses (A), orthotopic tumor burden (B and C), liver metastases (D), and survival analysis (E) in B-DNG mice (n = 6 mice per group). Scale bar, 2000 μm.

(**F-K**) Orthotopic implantation of OS-RC-2 cells with FOXA2 restoration for spontaneous lung metastasis analysis. Shown are BLI analyses (F), orthotopic tumor burden (G and H), lung metastases (I), liver metastases (J), and survival analysis (K) in B-DNG mice (n = 6 mice per group). Scale bar, 2000 μm.

Data are presented as mean ± SD. *p* values were determined with two-way ANOVA (A and F), two-tailed, unpaired Student's *t*-tests (B-D, and G-J), and log-rank test (E and K). $^{*}p < 0.05$. $^{**}p < 0.01$. $^{****}p < 0.001$.

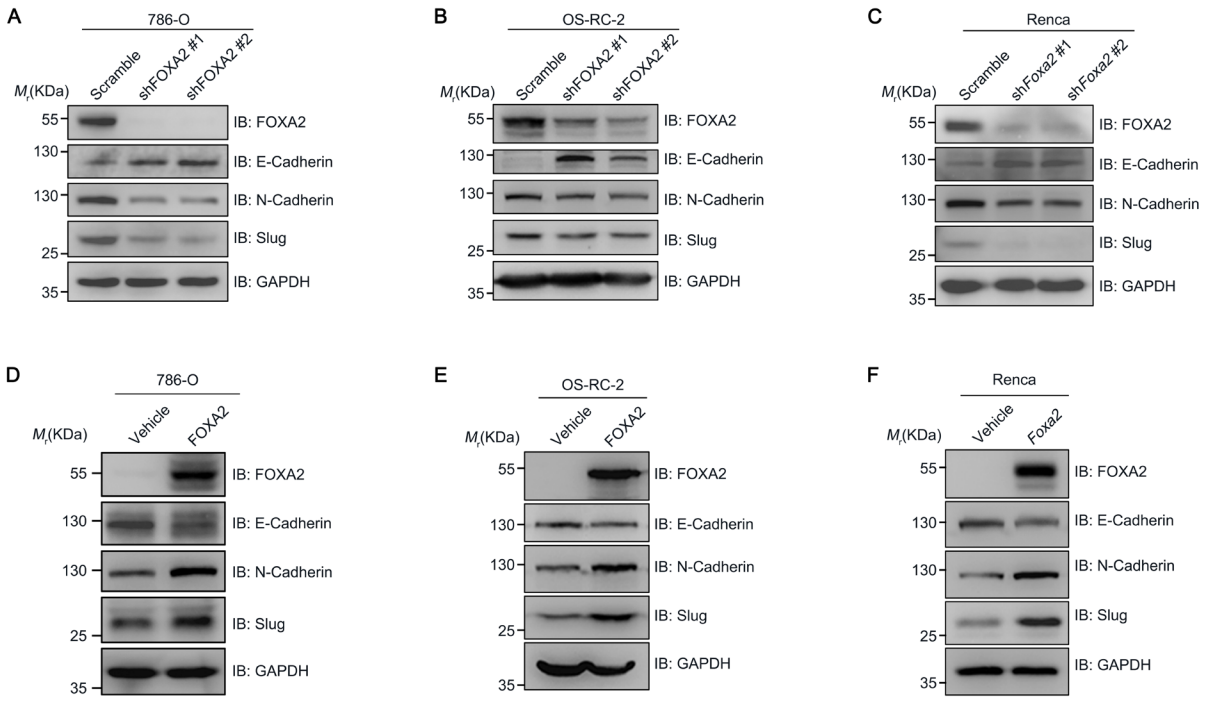


Figure S7. FOXA2 regulates EMT program in ccRCC.

(**A-C**) Western blotting analysis of epithelial-mesenchymal transition (EMT)-related markers E-Cadherin, N-Cadherin, and slug in 786-O (A), OS-RC-2 (B), and Renca (C) cells with or without FOXA2 knockdown.

(**D-F**) Western blotting analysis of EMT-related markers E-Cadherin, N-Cadherin, and slug in 786-O (D), OS-RC-2 (E), and Renca (F) cells with or without FOXA2 overexpression.

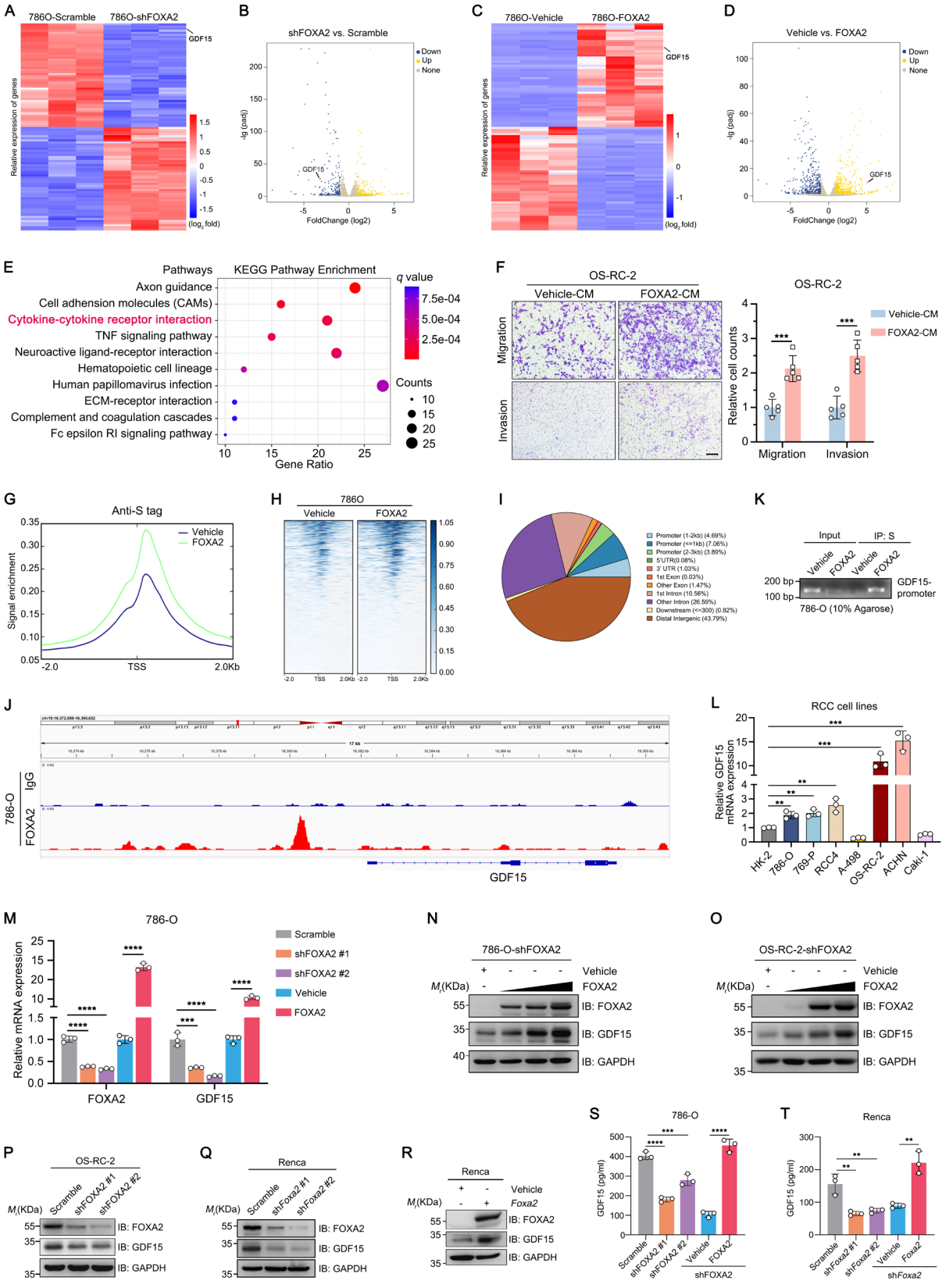


Figure S8. FOXA2 transcriptionally activates GDF15 expression.

(**A** and **B**) Heatmap (A) and volcano plot (B) showing the differentially expressed genes between scramble and FOXA2 knockdown 786-O cells.

(**C** and **D**) Heatmap (C) and volcano plot (D) showing the differentially expressed genes

between vehicle and FOXA2 overexpression 786-O cells.

(**E**) Kyoto Encyclopedia of Genes and Genomes (KEGG) analysis showing the top 10 enriched pathways in FOXA2 overexpression 786-O cells.

(**F**) Representative images (left) and quantification (right) of transwell migration and invasion assays in OR-RC-2 cells cocultured with conditioned medium (CM) derived from vehicle or FOXA2 overexpression ccRCC cells. Scale bar, 100 μm.

(**G** and **H**) Density plot (G) and heatmaps (H) of ChIP-seq signals for FOXA2 peaks in the transcription start site (TSS) region in 786-O cells.

(**I**) Pie chart showing the genomic distribution of FOXA2 binding peaks in 786-O cells.

(**J**) ChIP-seq using anti-FOXA2 antibody showing endogenous FOXA2 occupancy at the GDF15 genomic loci in parental 786-O cells.

(**K**) ChIP-PCR analysis using anti-S-tag antibody for FOXA2 enrichment on the GDF15 promoter in 786-O cells.

(**L**) RT-qPCR analysis of GDF15 mRNA expression in HK-2 and various RCC cell lines.

(**M**) RT-qPCR analysis of GDF15 mRNA expression in 786-O cells with FOXA2 knockdown or overexpression.

(**N** and **O**) Western blotting analysis of GDF15 levels in vehicle and FOXA2 overexpression 786-O (N) or OS-RC-2 (O) cells.

(**P**) Western blotting analysis of GDF15 protein levels in OS-RC-2 cells with FOXA2 knockdown.

(**Q** and **R**) Western blotting analysis of GDF15 protein levels in Renca cells with FOXA2 knockdown (Q) or overexpression (R).

(**S** and **T**) ELISA quantification of secreted GDF15 in the CM derived from 786-O (S) and Renca (T) cells with FOXA2 knockdown or overexpression.

Data are presented as mean ± SD. *p* values were determined with two-tailed, unpaired Student's *t*-tests (F and L) and one-way ANOVA followed by Dunnett's multiple-comparison test (M, S, and T). $^{**}p < 0.01$. $^{***}p < 0.001$. $^{****}p < 0.0001$.

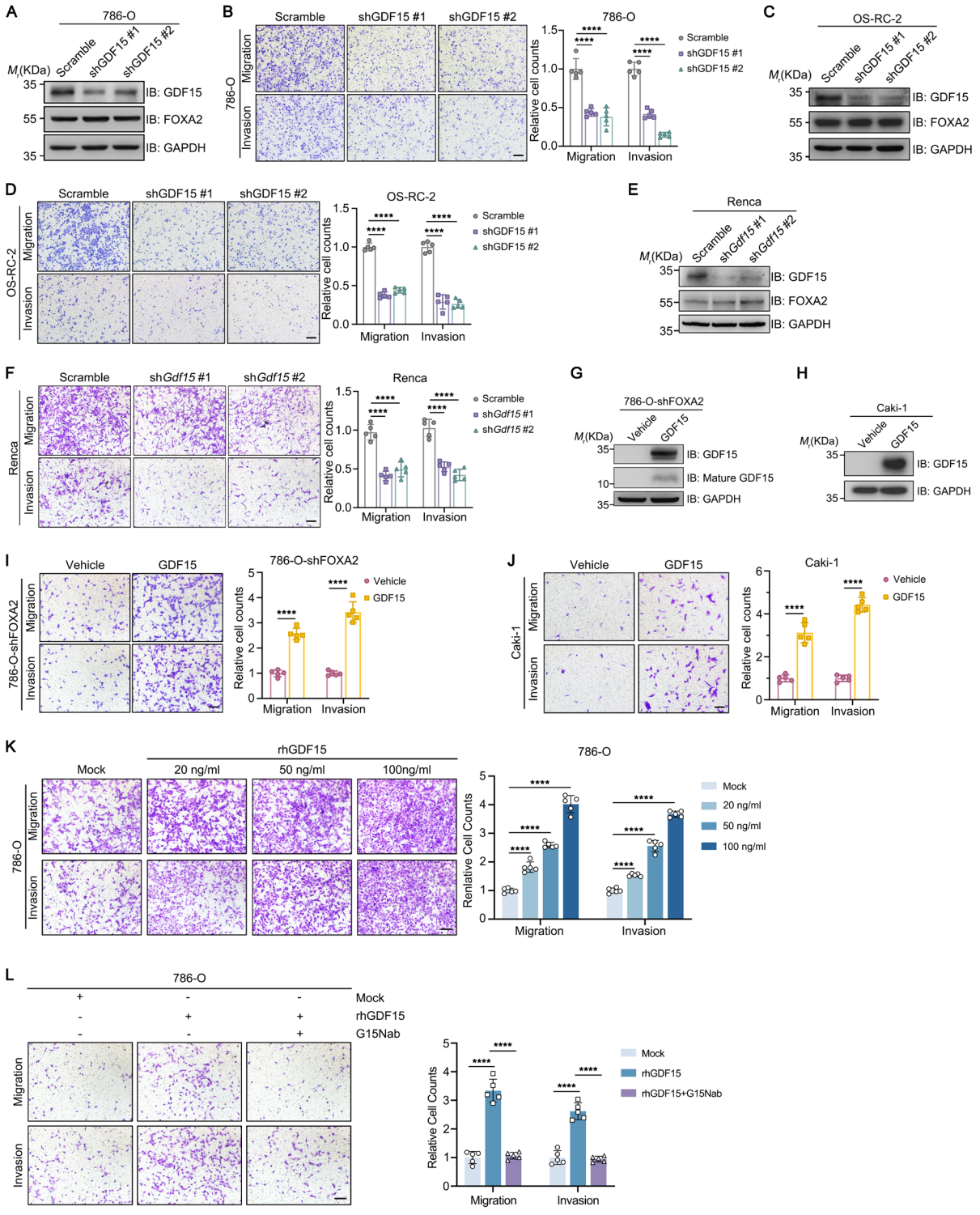


Figure S9. GDF15 promotes ccRCC metastasis *in vitro*.

(**A**) Western blotting analysis for the efficiency of GDF15 knockdown in 786-O cells.

(**B**) Representative images (left) and quantification (right) of transwell migration and invasion assays in scramble or GDF15 knockdown 786-O cells. Scale bar, 100 μm.

(**C**) Western blotting analysis for the efficiency of GDF15 knockdown in OS-RC-2 cells.

(**D**) Representative images (left) and quantification (right) of transwell migration and invasion assays in scramble or GDF15 knockdown OS-RC-2 cells. Scale bar, 100 μm.

(**E**) Western blotting analysis for the efficiency of *Gdf15* knockdown in Renca cells.

(**F**) Representative images (left) and quantification (right) of transwell migration and invasion assays in scramble or *Gdf15* knockdown Renca cells. Scale bar, 100 μm.

(**G** and **H**) Western blotting analysis for the efficiency of GDF15 overexpression in 786-O (G) and Caki-1 (H) cells.

(**I** and **J**) Representative images (left) and quantification (right) of transwell migration and invasion assays in vehicle or GDF15 overexpression 786-O (I) and Caki-1 (J) cells. Scale bar, 100 μm.

(**K**) Representative images (left) and quantification (right) of transwell migration and invasion assays in 786-O cells treated with increasing concentrations of recombinant human GDF15 (rhGDF15). Scale bar, 100 μm.

(**L**) Representative images (left) and quantification (right) of transwell migration and invasion assays in 786-O cells treated with 50 ng/ml rhGDF15, with or without GDF15 neutralizing antibody (G15Nab). Scale bar, 100 μm.

Data are presented as mean ± SD. *p* values were determined with one-way ANOVA followed by Dunnett's multiple-comparison test (B, D, F, K, and L) and two-tailed, unpaired Student's *t*-tests (I and J). $^{****}p < 0.0001$.

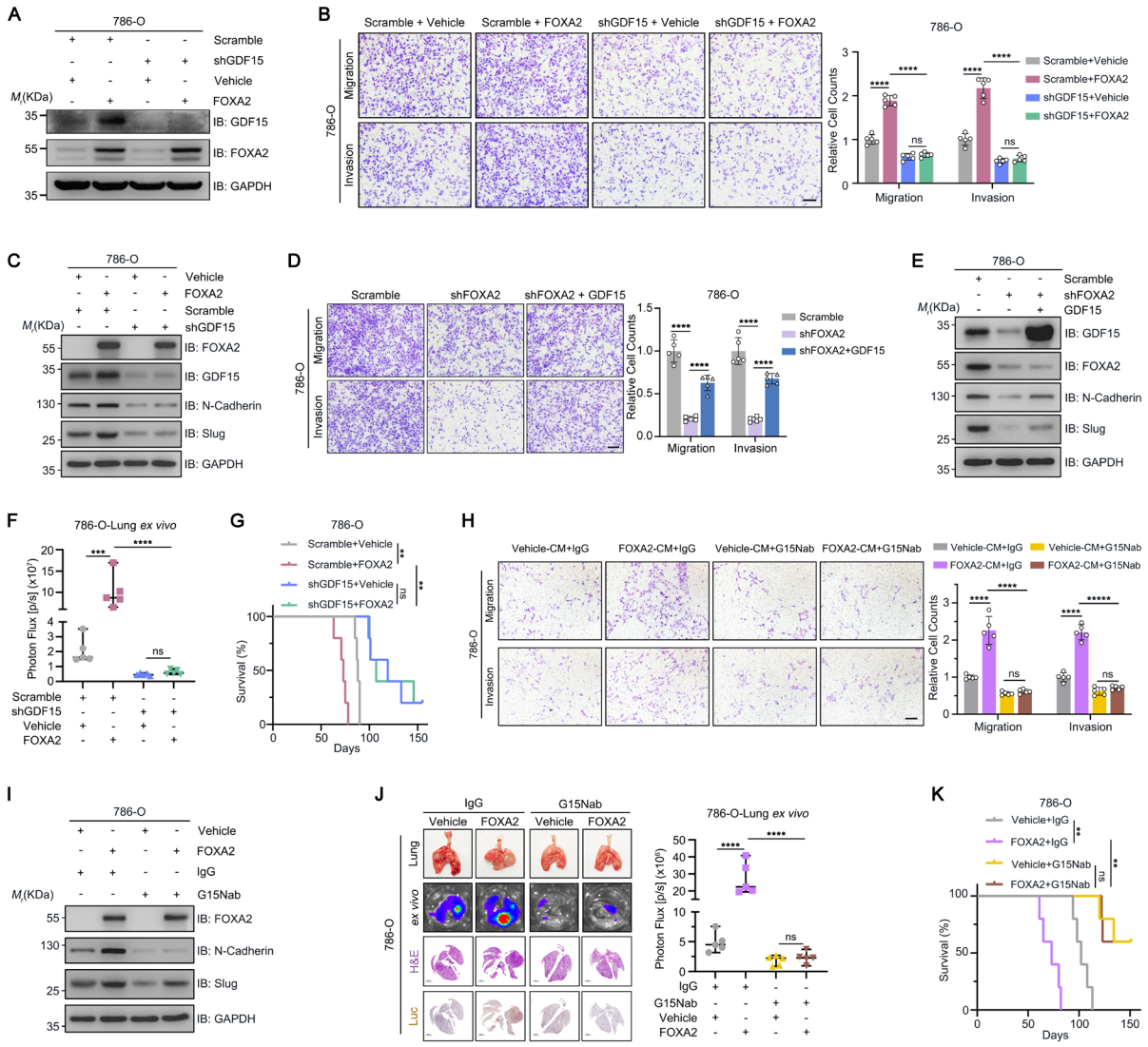


Figure S10. Tumor-derived GDF15 mediates FOXA2-induced 786-O cell metastasis.

(**A**) Western blotting analysis for the efficiency of FOXA2 overexpression and GDF15 knockdown in 786-O cells.

(**B**) Representative images (left) and quantification (right) of transwell migration and invasion assays in 786-O cells overexpressing vehicle or FOXA2, with or without GDF15 knockdown. Scale bar, 100 μm.

(**C**) Western blotting analysis of EMT-related markers N-Cadherin and Slug in 786-O cells overexpressing vehicle or FOXA2, with or without GDF15 knockdown.

(**D**) Representative images (left) and quantification (right) of transwell migration and invasion assays in FOXA2 knockdown 786-O cells, with or without GDF15 overexpression. Scale bar, 100 μm.

(**E**) Western blotting analysis of EMT-related markers N-Cadherin and Slug in FOXA2 knockdown 786-O cells, with or without GDF15 overexpression.

(**F**) Quantification of lung *ex vivo* bioluminescence from B-NDG mice intravenously injected with 786-O cells overexpressing FOXA2 or vehicle control, with or without GDF15 knockdown (n = 5 mice per group).

(**G**) Survival analysis of B-NDG mice after intravenous injection of indicated 786-O cells (n = 5 mice per group).

(**H**) Representative images (left) and quantification (right) of transwell migration and invasion assays in 786-O cells overexpressing vehicle or FOXA2, cocultured with IgG or G15Nab. Scale bar, 100 μm.

(**I**) Western blotting analysis of EMT-related markers N-Cadherin and slug in 786-O cells overexpressing vehicle or FOXA2, cocultured with IgG or G15Nab.

(**J**) Representative lung *ex vivo* BLI analyses (left) and quantification of lung photon flux (right) from B-NDG mice intravenously injected with 786-O cells overexpressing FOXA2 or vehicle control, followed by treatment with IgG or G15Nab (n = 5 mice per group). Scale bar, 2000 μm.

(**K**) Survival analysis of B-NDG mice injected intravenously with vehicle or FOXA2 overexpression 786-O cells, followed by administrated with IgG or G15Nab (n = 5 mice per group).

Data are presented as mean ± SD. *p* values were calculated using one-way ANOVA followed by Tukey's multiple-comparison test (B, D, F, H, and J) and log-rank test (G and K). $^{**}p < 0.01$. $^{***}p < 0.001$. $^{****}p < 0.0001$. ns, not significant.

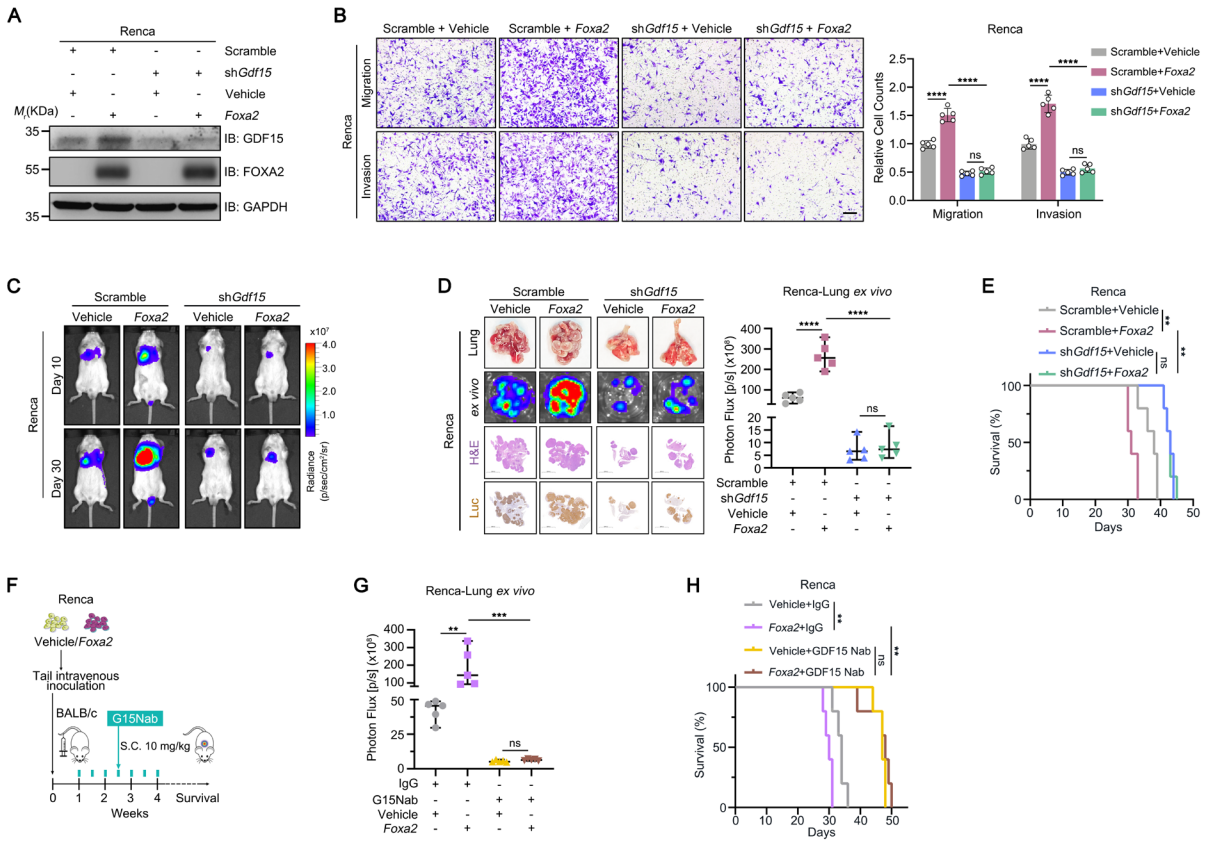


Figure S11. Tumor-derived *Gdf15* mediates *Foxa2*-induced Renca cell metastasis.

(**A**) Western blotting analysis for the efficiency of *Foxa2* overexpression and *Gdf15* knockdown in Renca cells.

(**B**) Representative images (left) and quantification (right) of transwell migration and invasion assays in Renca cells overexpressing *Foxa2* or vehicle control, with or without *Gdf15* knockdown. Scale bar, 100 μm.

(**C-E**) Intravenous injection of Renca cells with *Foxa2* overexpression with or without *Gdf15* knockdown for lung metastasis analysis. Shown are representative bioluminescence images (C), lung metastases (D), and survival analysis (E) of the BALB/c mice (n = 5 mice per group). Scale bar, 2000 μm.

(**F**) Schematic illustration of BALB/c mice intravenously injected with Renca cells overexpressing *Foxa2* or vehicle control, followed by IgG or G15Nab administration.

(**G**) Quantification of lung *ex vivo* bioluminescence from BALB/c mice intravenously injected with Renca cells overexpressing *Foxa2* or vehicle control, followed by treatment with G15Nab (n = 5 mice per group).

(**H**) Survival analysis of BALB/c mice injected intravenously with vehicle or *Foxa2* overexpression Renca cells, followed by administrated with IgG or G15Nab (n = 5 mice per group).

Data are presented as mean ± SD. *p* values were calculated using one-way ANOVA followed by Tukey's multiple-comparison test (B, D, and G) and log-rank test (E and H). $^{**}p < 0.01$. $^{***}p < 0.001$. $^{****}p < 0.0001$. ns, not significant.

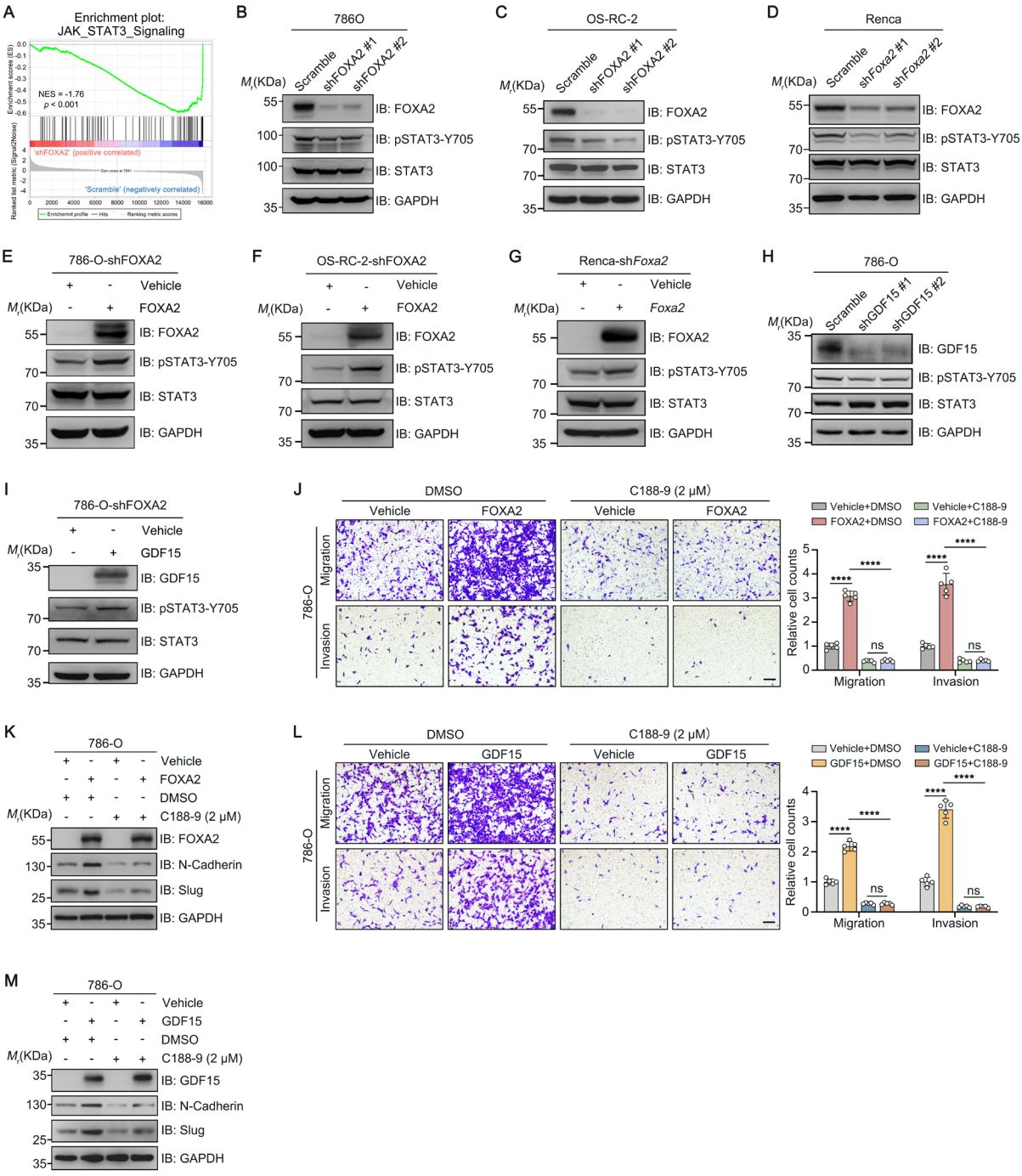


Figure S12. FOXA2 promotes GDF15-mediated STAT3 activation to facilitate ccRCC metastasis.

(**A**) Gene Set Enrichment Analysis (GSEA) plot of the STAT3 signaling in FOXA2 knockdown versus scramble 786-O cells.

(**B-D**) Western blotting analysis of pSTAT3-Y705 expression in 786-O (B), OS-RC-2 (C), and Renca (D) cells with or without FOXA2 knockdown.

(**E-G**) Western blotting analysis of pSTAT3-Y705 expression in 786-O (E), OS-RC-2 (F), and Renca (G) cells with or without FOXA2 overexpression.

(**H** and **I**) Western blotting analysis of pSTAT3-Y705 expression in 786-O cells with GDF15 knockdown (H) or overexpression (I).

(**J**) Representative images (left) and quantification (right) of transwell migration and invasion assays in 786-O cells overexpressing FOXA2 or vehicle control, treated with either DMSO or the STAT3 inhibitor C188-9. Scale bar, 100 μm.

(**K**) Western blotting analysis of EMT-related markers N-Cadherin and Slug in 786-O cells overexpressing FOXA2 or vehicle control, treated with either DMSO or the STAT3 inhibitor C188-9.

(**L**) Representative images (left) and quantification (right) of transwell migration and invasion assays in 786-O cells overexpressing GDF15 or vehicle control, treated with either DMSO or the STAT3 inhibitor C188-9. Scale bar, 100 μm.

(**M**) Western blotting analysis of EMT-related markers N-Cadherin and Slug in 786-O cells overexpressing GDF15 or vehicle control, treated with either DMSO or the STAT3 inhibitor C188-9.

Data are presented as mean ± SD. *p* values were calculated using one-way ANOVA followed by Tukey's multiple-comparison test (J and L). $^{****}p < 0.0001$.

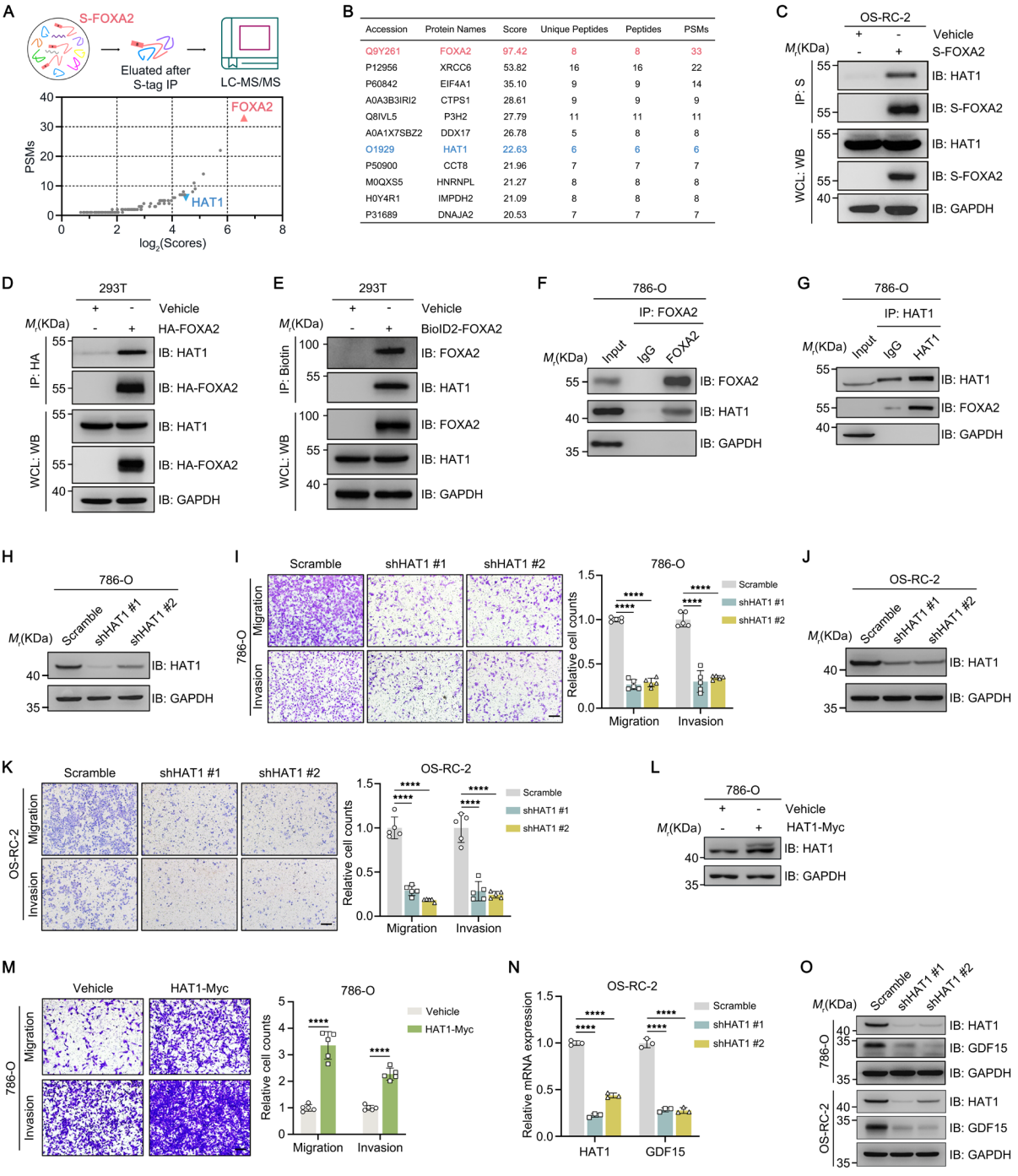


Figure S13. HAT1 promote ccRCC cell metastasis *in vitro*.

(**A**) Schematic illustration of pull-down assay using anti-S agarose in 786-O cells transfected with vehicle or S-FOXA2, followed by liquid chromatography–mass spectrometry (LC-MS) analysis.

(**B**) Protein interacting with FOXA2 identified by LC-MS analysis.

(**C**) Co-Immunoprecipitation (Co-IP) analysis of S-FOXA2 and HAT1 using anti-S in OS-RC-2 cells stably transfected with S-FOXA2 or vehicle control.

(**D**) Co-IP analysis of HA-FOXA2 and HAT1 using anti-HA in 293T cells transiently transfected with HA-FOXA2 or vehicle control.

(**E**) Co-IP analysis of BioID2-FOXA2 and HAT1 using streptavidin pull-down in 293T cells

expressing BioID2-FOXA2 or vehicle control.

(**F**) Co-IP analysis of endogenous FOXA2 and HAT1 in 786-O cells using anti-FOXA2 or IgG control.

(**G**) Co-IP analysis of endogenous HAT1 and FOXA2 in 786-O cells using anti-HAT1 or IgG control.

(**H**) Western blotting analysis for the efficiency of HAT1 knockdown in 786-O cells.

(**I**) Representative images (left) and quantification (right) of transwell migration and invasion assays in scramble or HAT1 knockdown 786-O cells. Scale bar, 100 μm.

(**J**) Western blotting analysis for the efficiency of HAT1 knockdown in OS-RC-2 cells.

(**K**) Representative images (left) and quantification (right) of transwell migration and invasion assays in scramble or HAT1 knockdown OS-RC-2 cells. Scale bar, 100 μm.

(**L**) Western blotting analysis for the efficiency of HAT1 overexpression in 786-O cells.

(**M**) Representative images (left) and quantification (right) of transwell migration and invasion assays in vehicle or HAT1 overexpression 786-O cells. Scale bar, 100 μm.

(**N**) RT-qPCR analysis of HAT1 and GDF15 mRNA expression in OS-RC-2 cells with or without HAT1 knockdown.

(**O**) Western blotting analysis of HAT1 and GDF15 expression in ccRCC cells with or without HAT1 knockdown.

Data are presented as mean ± SD. *p* values were determined with one-way ANOVA followed by Dunnett's multiple-comparison test (I, K, and N) and two-tailed, unpaired Student's *t*-tests (M). $^{****}p < 0.0001$.

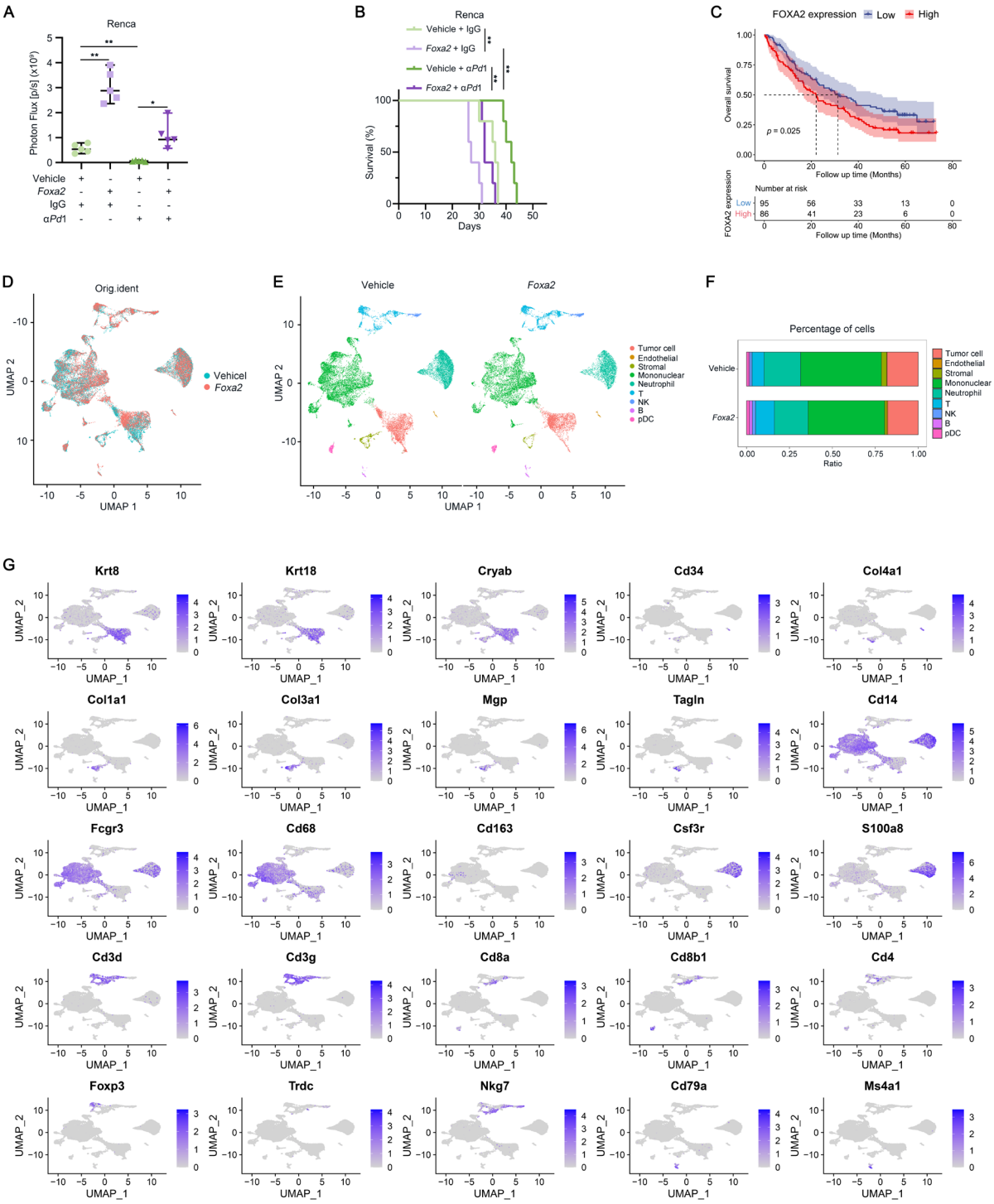


Figure S14. FOXA2 overexpression correlates with resistance to anti-PD-1 therapy.

(**A**) Quantification of lung *ex vivo* bioluminescence from BALB/c mice intravenously injected with Renca cells overexpressing *Foxa2* or vehicle control, followed by treatment with anti-PD-1 (n = 5 mice per group).

(**B**) Survival analysis of BALB/c mice injected intravenously with vehicle or *Foxa2* overexpression Renca cells, followed by administration with anti-PD-1 (n = 5 mice per group).

(**C**) Kaplan-Meier analyses for overall survival in ccRCC patients treated with anti-PD-1 therapy, stratified by FOXA2 expression.

(**D**) Uniform Manifold Approximation and Projection (UMAP) plots of single cells identified

by scRNA-seq and colored by the experimental groups.

(**E**) UMAP plots of scRNA-seq profiles from lung metastases derived from vehicle or *Foxa2* overexpression Renca cells, colored by the major cellular populations.

(**F**) Bar plot quantification of major cellular populations in lung metastasis derived from vehicle or *Foxa2* overexpression Renca cells.

(**G**) UMAP plots depicting the normalized expression patterns of selected marker genes across different cell populations.

Data are presented as mean ± SD. *p* values were calculated using one-way ANOVA followed by Tukey's multiple-comparison test (A) and log-rank test (B and C). $^{*}p < 0.05$. $^{**}p < 0.01$.

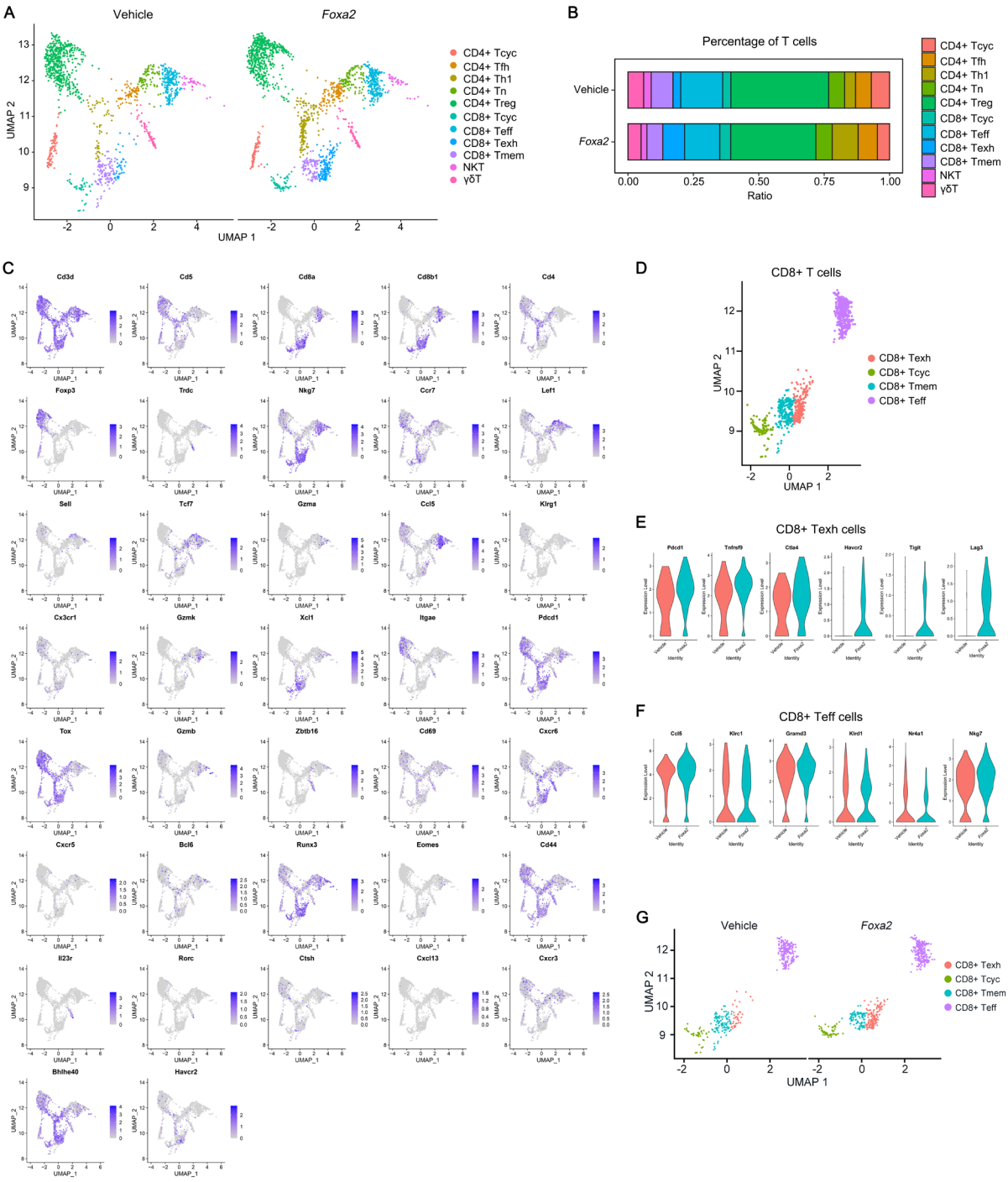


Figure S15. FOXA2 overexpression is associated with CD8$^+$ T cell exhaustion.

(**A**) UMAP plots of T cells from lung metastases in vehicle and *Foxa2* overexpression groups, colored by the T cell subtypes.

(**B**) Bar plot quantification of T cell types in lung metastases derived from vehicle or *Foxa2* overexpression Renca cells.

(**C**) UMAP plots depicting normalized expression of canonical lineage markers across T cell subsets.

(**D**) UMAP plots of CD8$^+$ T cells colored by the major cellular populations.

(**E** and **F**) Violin plots for the indicated gene signatures in CD8$^+$ Texh (F) and Teff (G) cells.

(**G**) Distribution of CD8$^+$ T cell subpopulations in lung metastasis derived from vehicle or *Foxa2* overexpression Renca cells.

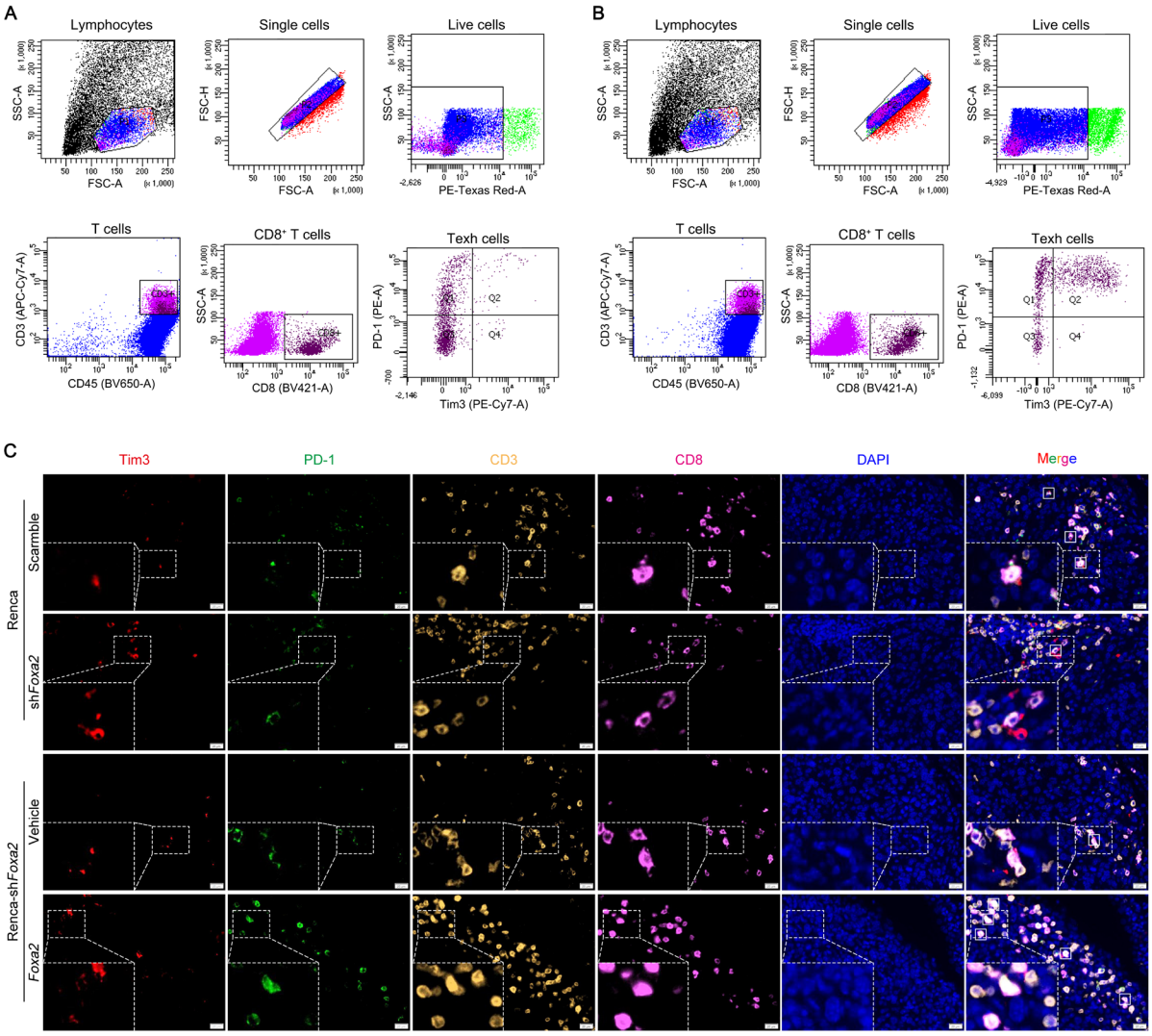


Figure S16. Gating strategy and mIHC staining for tumor-infiltrating CD8⁺ T cells.

(**A** and **B**) Shown are representative flow cytometry plots illustrating the gating strategy used to identify CD8⁺ T cells from lung metastatic tumors derived from mice injected with vehicle control (A) or *Foxa2* overexpression Renca cells (B).

(**C**) Representative multiplex immunohistochemistry (mIHC) staining for Tim3 (red), PD-1 (green), CD3 (orange), CD8 (purple), and DAPI (blue). Scale bar: 20 μm.

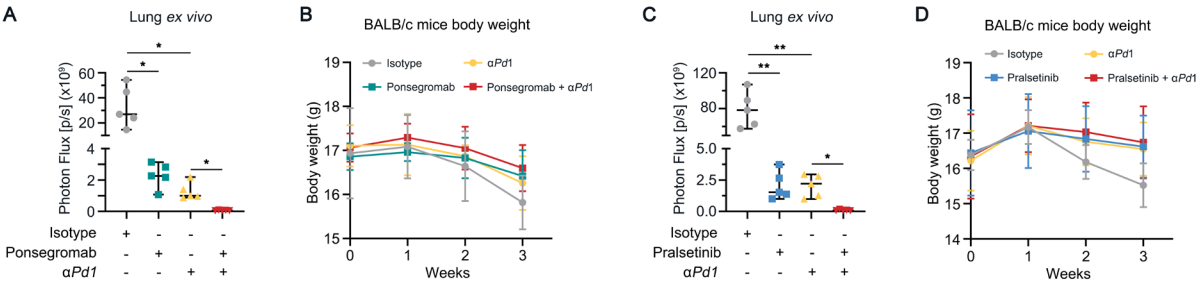


Figure S17. Blocking FOXA2-GDF15 axis synergizes with anti-PD-1 therapy in metastatic ccRCC.

(**A** and **B**) Intravenous injection of Renca cells followed by administration with isotype control, ponsegromab, and/or anti-PD-1 (n = 5 mice per group). Shown are quantification of lung *ex vivo* photon flux (A) and body weight changes during treatment (B).

(**C** and **D**) Intravenous injection of Renca cells followed by administration with isotype control, pralsetinib, and/or anti-PD-1 (n = 5 mice per group). Shown are quantification of lung *ex vivo* photon flux (C) and body weight changes during treatment (D).

Data are presented as mean ± SD. *p* values were calculated using one-way ANOVA followed by Tukey's multiple-comparison test (A and C). $^{*}p < 0.05$. $^{**}p < 0.01$.

Supplemental Methods

Clinical specimens

Tumors and adjacent normal tissues (NATs), designated as cohort 1, were collected from 275 patients diagnosed with clear cell renal cell carcinoma (ccRCC) at Peking University First Hospital (PKUFH) between January 10, 2007, and December 29, 2010. Primary tumor tissues and matched distant metastatic lesions, defined as cohort 2, were obtained from 117 patients with pathologically confirmed metastatic ccRCC who underwent surgical resection without prior anticancer therapy from November 13, 2012, to May 20, 2025. Additionally, cohort 3 comprised 86 formalin-fixed, paraffin-embedded (FFPE) ccRCC tumor specimens obtained from patients undergoing nephrectomy between January 10, 2007, and March 9, 2009. All hematoxylin and eosin (H&E) slides were independently reviewed and confirmed by two experienced pathologists. Detailed clinical and pathological data were retrieved from electronic medical records.

Immunohistochemistry and scoring

Immunohistochemistry (IHC) staining were performed as previously described. Briefly, FFPE ccRCC tissues were sectioned at 4 μm thickness. Slides were dried at 70°C for 1 h, followed by deparaffinization in dimethylbenzene and rehydration through a graded ethanol series. Antigen retrieval was conducted using citrate retrieval buffer (PH 6.0) under high pressure for 10 min. Endogenous peroxidase activity was quenched with 0.3% hydrogen peroxide for 15 min at room temperature. Slides were then incubated overnight at 4°C with primary antibodies, including FOXA2 (1:200, Santa Cruz, sc-101060), GDF15 (1:50, Abcam, ab206414), and HAT1 (1:500, Abcam, ab194296). Subsequently, sections were incubated with appropriate secondary antibodies for 1 h at room temperature. The immune complexes were visualized using the 3,3’-diaminobenzidine tetrahydrochloride (DAB), and nucleus were counterstained with hematoxylin.

For quantification, slides were evaluated independently and blindly by two pathologists. The staining intensity were scored as 0 for no staining, 1 for weak staining, 2 for medium staining, and 3 for strong staining. The proportion of positive cells were quantified as followed: 0 for < 5% positive cells, 1 for 5-25% positive cells, 2 for 26-50% positive cells, 3 for 51-75% positive cells, and 4 for > 75% positive cells. The IHC score was calculated by multiplying the intensity and proportion of positive cells (range, 0–12). Based on the IHC score, target protein staining was categorized as negative (0–3), weak (4–6), moderate (7–9), or strong (10–12). Patients were further stratified into high- and low- expression groups using an IHC score cutoff of 7.

Bioinformatics analysis

Publicly available metastatic ccRCC microarray datasets of GSE22541 were downloaded from the Gene Expression Omnibus (GEO) database (http://www.ncbi.nlm.nih.gov/geo). Genomic and clinical profiles from The Cancer Genome Atlas-Kidney Renal Clear Cell Carcinoma (TCGA-KIRC) cohort were downloaded from the web portal (https://cancergenome.nih.gov/). Clinical information and RNA-seq expression data of advanced ccRCC patients treated with anti-PD-1 antibody nivolumab were obtained from a previously published study (https://www.nature.com/articles/s41591-020-0839-y#Sec8). Differentially expressed genes (DEGs) were identified using the DESeq2 package in R (https://www.r-project.org). Genes with an adjusted p value < 0.05 and $|\log_2$ fold-change$|$ > 1 were considered differentially expressed. For survival analysis, patients were categorized into high and low expression groups based on the median (50th percentile) expression level of FOXA2. Kaplan-Meier analyses were used to explore the association between FOXA2 mRNA expression and clinical outcomes.

Cell lines and cell culture

Human embryonic kidney cells (HEK293T), human immortalized renal epithelial cells (HK-2), human RCC cell lines (786-O, OS-RC-2, 769-P, RCC4, A-498, ACHN, and Caki-1), and the murine renal cancer cells (Renca) were originally obtained from the American Type Culture

Collection (ATCC). HEK293T, RCC4, and A-498 cells were cultured in Dulbecco's Modified Eagle Medium (Gibco, C11995500BT), 786-O, OS-RC-2, 769-P, and ACHN cells were cultured in RPMI-1640 medium (Corning, 10-040-CVRC), HK-2 cells were cultured in keratinocyte serum-free medium (Gibco, 17005-042), and Caki-1 cells were cultured in McCoy's 5A Medium (Gibco, 16600082). The media were all supplemented with 10% heat-inactivated fetal bovine serum (FBS; Gibco, 10099141). All cell lines were authenticated by short tandem repeat analysis and routinely tested to confirm absence of mycoplasma contamination. All cells were cultured aseptically at 37℃ in humidified atmospheres with 5% CO_2. For conditioned media (CM) experiments, culture supernatants were collected after 48 h from cells grown in complete medium (containing 10% FBS), centrifuged to remove debris, and mixed 1:1 with fresh complete RPMI-1640 medium prior to use in subsequent assays.

Plasmid constructs

Short hairpin RNA (shRNA) sequences targeting FOXA2, *Foxa2*, GDF15, and HAT1 were designed using the online shRNA designer tool (https://portals.broadinstitute.org/gpp/public/), and inserted into pLKO.1-TRC vector (Addgene, #10878). The specific shRNA target sequences are listed in **Supplemental Table 1**. Full-length human FOXA2 was amplified from HEK293T cell cDNA and cloned into pLVX-IRES-Bla vector (with an N-terminal HAS tag) or myc-BioID2-MCS vector. GDF15 and HAT1 were constructed into pLVX-Bla and pCDH-Hygro vectors, respectively. The murine *Foxa2* was amplified from Renca cells and inserted into pLVX-Bla vector. The promoter regions of GDF15 were subcloned into pGL4.10-luc2 luciferase reporter vector (Promega, E6651). All plasmid constructs were confirmed by Sanger DNA sequencing.

Lentiviral infection and plasmid transfection

Lentivirus transduction was performed to generate individual stable cell lines for gene overexpression or shRNA-mediated knockdown, with empty vector used as the controls.

Targeted cells were incubated with lentivirus for 24 h in the presence of 10 μg/mL polybrene (Santa Cruz, sc-134220). Infected cells were then selected using 1.0 μg/mL puromycin, 2.0 μg/mL blasticidin, or 1.0 μg/mL hygromycin, as appropriate, until uninfected control cells were completely eliminated. Transient plasmid transfections were performed using Lipofectamine 3000 reagent (Thermo Fisher Scientific, L3000015) according to the manufacturer's instructions.

Generation of CRISPR/Cas9 KO cell lines

Single-guide RNAs (sgRNAs) targeting the FOXA2 gene were designed using the online CRISPR design program CRISPick (https://portals.broadinstitute.org/gppx/crispick/public) and cloned into BsmBI-linearized lentiCRISPRv2 vector (Addgene, #52961). The sgRNA target sequences of FOXA2 are listed in **Supplemental Table 1**. Lentiviral particles were generated by co-transfecting HEK293T cells with the lentiCRISPRv2-sgRNA plasmid and packaging vectors. To construct FOXA2-konckout (KO) cells, target cells were infected with CRISPR-Cas9-sgRNA lentivirus and selected with puromycin (1.0 μg/mL). Single puromycin-resistant clones were isolated and the KO efficiency was validated by western blotting.

RNA extraction and quantitative RT-PCR

Total RNA was extracted using TRIzol reagent (Invitrogen, 15596018) following the manufacturer's instructions. First-strand cDNA was synthesized with 1 μg of total RNA using the TransScript All-in-One First-Strand cDNA Synthesis Kit (Transgen, AT341). The cDNA samples used for gene expression analysis were diluted by 1:20. Quantitative reverse transcription PCR (RT-PCR) was conducted in triplicate on 96-well optical plates using Applied Biosystems 7500 Real-Time PCR System (Thermo Fisher Scientific) and SYBR Green PCR Master Mix (Transgen, AQ131) according to the manufacturer's instructions. The α-tubulin was used as the endogenous control for normalization. The primers used in this study are showed in **Supplemental Table 2**.

Western blot analysis

Cultured cells were lysed in ice-cold lysis buffer (50 mM Tris-HCl, 150 mM NaCl, 1% NP-40 detergent, 0.5% sodium deoxycholate, and 0.1% SDS) supplemented with protease and phosphatase inhibitor cocktails (Cell Signaling Technology, 5872). Lysates were cleared by centrifugation at 16000g for 30 min at 4 °C. Protein concentrations were measured using the BCA Protein Assay Kit (Thermo Fisher Scientific, 23225). Total proteins were separated by SDS-PAGE on 8-12% gels and transferred to 0.45 μm polyvinylidene fluoride (PVDF) membranes (Millipore, IPVH00010). Membranes were blocked with 5% nonfat dry milk in Tris-buffered saline containing 0.1% Tween (TBS-T) for 1 h at room temperature and then incubated with specific primary antibodies at 4°C overnight. After washing with TBS-T, membranes were incubated with HRP-conjugated goat anti-mouse (Immunoway, RS0001) or anti-rabbit (Immunoway, RS0002) secondary antibodies (1:10000) accordingly. The immune bands were visualized by the Genesys G:Box iChemi XL imaging system. All primary antibodies used in this study are listed in **Supplemental Table 3**.

Transwell assay

Cell migration and invasion assays were performed using Transwell inserts with 8.0 μm pores polycarbonate membranes (Corning, 3422), and conducted with uncoated and coated Matrigel (Corning, 354234), respectively. Briefly, the indicated cells were seeded in the upper chambers containing 200 μL serum-free medium while the lower chambers contained 700 μL medium supplemented with 10% FBS. After incubation at 37°C for 12 h, the cells were fixed with 4% paraformaldehyde and stained with 0.5% crystal violet (Millipore, V5265). Cells on the upper surface of the membrane were gently removed with a cotton swab, and migrated or invaded cells on the lower surface of the membrane were imaged and counted under the microscope (Olympus CX31, Germany).

Mice

B-NDG (Stain name: NOD.CB17-Prkdcscid Il2rgtm1Bcgen/Bcgen) mice and the BALB/c mice (4-5 weeks old, male) were purchased from BIOCYTOGEN (Beijing, China) and Beijing Vital River Laboratory Animal Technology (Beijing, China), respectively. All mice were housed under specific pathogen-free conditions in the animal facility at PKUFH.

Animal studies

For the experimental lung metastasis model, 1×10^6 luciferase-labeled 786-O, OS-RC-2, or Caki-1 cells in 100 μL phosphate buffer saline (PBS) were intravenously injected via the tail vein into B-NDG mice. For syngeneic models, 5×10^4 luciferase-labeled Renca cells were injected into BALB/c mice. For the orthotopic implantation and spontaneous metastatic models, 1×10^6 luciferase-labeled 786-O or OS-RC-2 cells were resuspended in 20 mL Matrigel diluted 1:1 with serum-free medium and then orthotopically injected into the left kidney capsule of B-NDG mice. Tumor growth and distant metastasis were monitored using the IVIS Spectrum Imaging System (PerkinElmer). Mice were intraperitoneally injected with D-Luciferin (15mg/ml, Abcam, ab145164) at a dose of 10 uL/g body weight. At experimental endpoint, mice were euthanized, and lungs, kidneys, and livers were harvested for *ex vivo* bioluminescence imaging and further histological analysis.

***In vivo* drug administration**

For drug administration assays, mice were randomized into treatment groups following intravenous injection of ccRCC cells. The GDF15 neutralizing antibody ponsegromab (PF 06946860, MedChemExpress, HY-P99241) was administrated subcutaneously (S.P.) at 10 mg/kg twice per week starting after tumor cell incubation. Anti-PD-1 antibody (BioXCell, clone RMP1-14, BE0146) was administrated intraperitoneally (I.P.) at 10 mg/kg twice weekly after tumor implantation. The RET inhibitor pralsetinib (BLU-667, MedChemExpress, HY-112301) was treated I.P. at 20 mg/kg every other day beginning one week after tumor

intravenous injection. At the endpoint, mice were euthanized, and lungs were collected for *ex vivo* imaging using 300 mg/mL D-luciferin solution in 24-well plates.

Immunofluorescence staining

For immunofluorescence (IF) staining of murine lung tissues, lungs were perfused with 50 ml of PBS via the right ventricle until visibly free of blood. Tissues were rinsed with pre-chilled PBS, fixed in 4% paraformaldehyde for 1 h at 4℃ on a shaker, and dehydrated in 30% sucrose overnight. Samples were then embedded in optimum cutting temperature (O.C.T, Sakura, 4583) and frozen at -80℃. Tissues were sectioned at 4 μm thickness, washed twice with PBS, permeabilized in 0.2% Triton X-100 (Sigma-Aldrich, 9036-19-5) for 15 min, and blocked in PBS containing 5% bovine serum albumin (BSA) for 1 h. 4',6-diamidino-2-phenylindole (DAPI) was used for counterstaining the nuclei.

For IF staining of cells, ccRCC cells were plated in confocal dishes and cultured for 36 h. Cells were fixed with 4% paraformaldehyde for 15 min, permeabilized in 0.2% Triton X-100 for 15 min, and blocked with 5% BSA in PBS for 1h at room temperature. Subsequently, cells were incubated with mouse anti-FOXA2 (1:100, Santa Cruz, sc-101060) and rabbit anti-HAT1 (1:100, Abcam, ab194296) overnight at 4℃. After washing with cold PBS for three times, the dishes were incubated with appropriate Alexa Fluor 488 (Thermo Fisher Scientific, A-11008) or Alexa Fluor 594 (Thermo Fisher Scientific, A-11012) conjugated secondary antibodies (1:1000). Nuclei were counterstained with DAPI. All the IF images were captured using the laser scanning confocal microscopy (Leica SP8 STED 3X, Germany).

Bulk RNA-seq and data analysis

Total RNA was isolated from 786-O cells using the RNeasy mini kit (QIAGEN, 74104) following the manufacturer's instructions. After RNA quality controlling and library constructing, triplicate samples were subjected to sequence by Annoroad Gene Technology (Beijing, China). Raw RNA-seq reads were quality filtered and mapped to human reference

genome (GRCh38, National Center for Biotechnology Information) using HISAT2 (Hierarchical Indexing for Spliced Alignment of Transcripts 2). DEGs analysis were performed using the DEseq2 package (R foundation), with significance thresholds set at $|Log_2$ (fold change) $| > 1$ and false discovery rate (FDR) < 0.05. Identified DEGs were subjected to Gene Ontology (GO) and Kyoto Encyclopedia of Genes and Genomes (KEGG) pathway enrichment analysis using the Database for Annotation, Visualization and Integrated Discovery (DAVID) bioinformatics platform.

Gene set enrichment analysis

Gene set enrichment analysis (GSEA) were performed using the Hallmark gene sets from the Molecular Signatures Database (MsigDB H: https://www.gsea-msigdb.org/gsea/msigdb/human/genesets.jsp?collection=H). Signature genes were compared using GSEA to the ranked list of genes affected by the expression level of FOXA2. Genes were ranked by ‘‘Differ_of_classes’’ and permutation type was ‘gene set’ and other sets using the GSEA default. Gene sets with a nominal *p*-value < 0.05 were considered significantly enriched.

Chromatin Immunoprecipitation assay

The Chromatin Immunoprecipitation (ChIP) assay was performed using the SimpleChIP Plus Enzymatic Chromatin IP Kit (Cell Signaling Technology, 9005) according to the manufacturer’s instructions. Briefly, indicated cells were cross-linked with 1% formaldehyde, quenched with glycine, and lysed with membrane extraction buffer containing protease/phosphatase inhibitors. After concentrating, the pellet nuclei were digested by Micrococcal Nuclease at 37°C for 20 min. The pellets were then resuspended in IP dilution buffer and sonicated. Chromatin supernatants were proceeded to the immunoprecipitation with the appropriate antibodies overnight at 4°C. Antibody-bound chromatin complexes were captured with Protein A/G magnetic beads and sequentially washed with low-salt, high-salt, LiCl buffer, and elution buffer. The DNA-protein cross-links were reversed by RNase A and

proteinase K digestion, and the precipitated chromatin DNA was finally purified through spin columns.

ChIP-seq and data analysis

Eluted ChIP DNA were used for library construction with the TruePrep DNA Library Prep Kit V3 for Illumina (Vazyme, TD503), following the manufacturer's instructions. Libraries were sequenced on the Illumina NovaSeq sequencing system (paired-end, 2 × 150 bp) at Novogene (Beijing). To analyze ChIP-seq data, the sequencing reads were mapped to the hg38 reference genome by Bowtie2 (version 2.3.5.1) after quality control and adapter trimming. Reads with mapping quality (MAPQ) score lower than 30 or mapped to mitochondria genome were excluded. Duplicate reads were removed using Picard tools (https://broadinstitute.github.io/picard/). Peak calling was performed using the MACS (version 2.2.5) peak finding algorithm with 0.05 set as the *q* value cutoff. Peak distribution was conducted with the 'annotatePeaks.pl' function in Homer tool and ChIP-seq data were visualized by using Integrative Genomics Viewer (IGV, version 2.5.3).

ChIP qPCR analysis

ChIP enrichment was quantified by qPCR and normalized to input DNA, and results were expressed as the relative enrichment of the material precipitated by indicated antibody on target regions. The primer sequences used for ChIP-qPCR are listed in **Supplemental Table 2**. The percent input method was used to calculate enrichment using the following formula: percent Input = $100\% \times 2^{(\text{C[T] input sample} - \text{C[T] IP sample})}$.

ELISA

A total of 5×10^5 cells were seeded in each well of a 6-well plate and cultured for 48 h. The supernatants were then collected, centrifuged, and diluted 1:2 with serum-free medium. GDF15 concentrations in the medium were measured using a human GDF15 ELISA Kit (Proteintech,

KE00108) according to the manufacturer's instructions. Diluted samples were added to wells pre-coated with GDF15 antibody and incubated at 37℃ for 30 min. The absorbance of each well was measured at 450 nm using a microplate reader (Tecan Spark, Switzerland). GDF15 concentration were determined based on the standard curve.

Dual-luciferase reporter assay

HEK293T cells were seeded in 96-well plates at a density of 1×10^4 cells per well. After 24 h, cells were cotransfected with 100 ng of luciferase reporter plasmid (pGL4.10-Basic, pGL4.10-GDF15 promoter, or pGL4.10-mutant GDF15 promoter), 100 ng of expression plasmid (pLVX-Bla-FOXA2 or empty control), and 50 ng of pRL-TK Renilla luciferase plasmid. After 48 h, firefly and Renilla luciferase activities were measured using the Dual-Luciferase Reporter Assay System (Promega, E1910) following the manufacturer's instructions. Firefly luciferase activity was normalized to Renilla luciferase activity and reported as the relative luciferase activity.

Coimmunoprecipitation

Cells were homogenized in ice-cold NETN buffer (150 mM NaCl, 1 mM EDTA, 50 mM Tris-HCl, pH 7.4-7.5, 1.0% NP-40) supplemented with 1 mM phenylmethylsulfonyl fluoride (PMSF), protease inhibitors, and phosphatase inhibitors (MedChemExpress, HY-K0021). Lysates were sonicated, incubated on ice for 30 min, and centrifuged at 12,000 g for 30 min at 4°C. Supernatants were then incubated overnight at 4°C with either S-protein agarose (Millipore, 69704), Anti-HA agarose (Proteintech, 51064-2-AP), Anti-c-Myc agarose (Thermo Fisher Scientific, 20168), streptavidin magnetic beads (Thermo Fisher Scientific, 88816), anti-FOXA2, anti-HAT1, or control IgG. The Immunocomplexes were washed three times with NETN buffer, eluted in SDS sample buffer, and boiled at 95°C for 10 min. The precipitated proteins were subsequently analyzed by immunoblotting or mass spectrometry.

Silver staining

The eluents from Co-IP assays were examined using SDS-PAGE, followed by silver staining with the Pierce™ Silver Stain Kit (Thermo Scientific, 24612) according to the manufacturer's instructions. For protein identification, all differentially stained bands were excised and subjected to mass spectrometry.

Mass spectrometry

Liquid chromatography-tandem mass spectrometry (LC-MS/MS) was performed to identify FOXA2-interacting cofactors. Differentially stained protein bands excised from silver-stained SDS-PAGE gels were enzymatically dissociated to generate peptides. The peptides were separated using the nanoViper C18 analytical column and analyzed on the Q-Exactive mass spectrometer (Thermo Fisher Scientific) equipped with a nano-flex ion source. All peptide identifications were validated by manual interpretation of the MS/MS spectra.

Tumor dissociation and scRNA-seq

The lungs from two groups of vehicle mice and *Foxa2* mice (n = 4 per group) were harvested on day 21 after intravenous injection of Renca cells. The lung metastatic tumor foci were micro-dissected under a dissection microscope using fine-tipped forceps. Then, the tumors were rinsed in ice-cold PBS, minced thoroughly, and dissociated with the mouse dissociation kit (Miltenyi Biote, Germany) at 37°C for 1 h. Single-cell suspension were filtered through a 40 μm strainer and subjected to red blood cell lysis. Dead cells were removed using the EasySep Dead Cell Removal (Annexin V) Kit (STEMCELL Technologies, 17899), followed by hashtag staining and labeling. scRNA-seq libraries were generated using the Chromium Single Cell 3' Reagent Kit v3 (10 × Genomics). Cell suspensions were loaded onto the Chromium Single Cell Platform and added into Gel Bead-In Emulsions (GEMs). The final libraries were sequenced on an Illumina NovaSeq6000 instrument at Capitalbio technology (Beijing, China).

Gene expression quantification and quality control

The Raw sequence reads were initially assessed for quality using FastQC. The Cell Ranger (Version 2.1.1) was used to process, align, and summarized unique molecular identifier (UMI) counts against the mouse mm10 reference genome obtained from the University of California Santa Cruz (UCSC). Unfiltered raw count matrices were imported into R for further analysis using the Seurat (v3.0) package. Low-quality cells were filtered out based on the following criteria: < 200 or > 8000 total UMI counts, > 12% mitochondrial UMIs, or expression of < 250 genes. Subsequently, the filtered data were normalized using the SCTransform function, with regressing out total UMI counts and mitochondrial UMI percentage. The principal component analysis was computed. The top principal components were determined using the ElbowPlot function, and used for uniform manifold approximation and projection (UMAP) dimensionality reduction.

Cell clustering and annotation

Cell clustering was performed using the Seurat package (v3.0) and Harmony to correct for batch effects across sequencing runs. Dimensionality reduction and clustering were conducted using the RunHarmony(), RunUMAP(), FindNeighbors(), and FindClusters() functions. Cluster-specific genes were identified using the using the FindAllMarkers() function with the Wilcoxon rank-sum test, and clusters were defined based on the genes significantly upregulated in each population. Differential expression between specific populations was analyzed using the FindMarker() function with default parameters. The cell populations were annotated based on the marker gene analysis and canonical markers reported in the literature.

Flow cytometry

The lung metastatic tumors were picked, minced, further enzymatically dissociated by 1 mg/ml collagenase Type III (Sigma-Aldrich, C2139) and 0.1 mg/ml DNase I (Sigma-Aldrich, D7291) at 37℃ for 1 h. Following digestion, the resulting cell suspensions were filtered through a 70

mm nylon mesh, centrifuged, and resuspended in red blood cell lysis buffer for 5 h at room temperature. After quenching and centrifugation, cells were resuspended in PBS and counted using an automated cell counter. For flow cytometric analysis, cells were incubated with anti-CD16/32 antibody (BioLegend, 156603) to block FcR for 10 min, and then stained with fluorophore-conjugated antibodies for 30 min at 4℃. Samples were run on the LSRFortessa flow cytometer (BD Biosciences). Populations were visualized and quantified by the FlowJo software (Version 10.0.8).

Multiplex immunohistochemistry

Multiplex immunohistochemistry (mIHC) was performed on FFPE mouse lung tissue sections using the PANO 7-plex IHC kit (Panovue) according to the manufacturer's instructions. Briefly, slides were baked, dewaxed in xylene, and rehydrated through graded ethanol. Antigen retrieval was performed in EDTA buffer (pH 9.0) by microwave heating. After incubation with blocking buffer (Panovue, 10018001120), sections were sequentially incubated with the primary antibodies against Tim3 (1:200, Cell Signaling Technology, 83882), PD-1 (1:100, Cell Signaling Technology, 84651), CD3 (1:100, Abcam, ab16669), and CD8α (1:100, Cell Signaling Technology, 98941). Each primary antibody incubation was followed by incubation with an HRP-conjugated secondary antibody (Panovue, 10013001050) and tyramide signal amplification (TSA). Microwave treatment was performed between staining cycles for antibody stripping and antigen retrieval. Nuclei were counterstained with DAPI. Stained slides were scanned using an Olympus VS200 (Olympus, Germany) equipped with an Olympus UPLXAPO 20× objective lens. Images analysis was conducted using QuPath software.

Supplemental Table 1. shRNA and sgRNA sequences used in the study.

Target	**Forward Sequence (5'-3')**	**Reverse Sequence (5'-3')**
Scramble	TTCTCCGAACGTGTCACGTAT	ATACGTGACACGTTCGGAGAA
shFOXA2 #1	CAGGTCTCGGGTCCGATTAAT	ATTAATCGGACCCGAGACCTG
shFOXA2 #2	GAACGGCATGAACACGTACAT	ATGTACGTGTTCATGCCGTTC
sh*Foxa2* #1	ATGAATGGCATGAACACATAC	GTATGTGTTCATGCCATTCAT
sh*Foxa2* #2	CAGGTCTCGGGTCTGATTTAA	TTAAATCAGACCCGAGACCTG
shGDF15 #1	CTGATGGAACTGTGTATTTAT	ATAAATACACAGTTCCATCAG
shGDF15 #2	CACTCCGAAGACTCCAGATTC	GAATCTGGAGTCTTCGGAGTG
shHAT1 #1	CATAGATACTACACTGAATTT	AAATTCAGTGTAGTATCTATG
shHAT1 #2	TGTAGAGGCTTTCGAGAATAT	ATATTCTCGAAAGCCTCTACA
sgFOXA2 #1	TCCGTGAGCAACATGAACGC	GCGTTCATGTTGCTCACGGAC
sgFOXA2 #2	CACGTACATGAGCATGTCGG	CCGACATGCTCATGTACGTGC

Supplemental Table 2. Primers used in this study.

qPCR primer	**Forward Sequence (5'-3')**	**Reverse Sequence (5'-3')**
FOXA2	GCACTCGGCTTCCAGTATGCT	CGTTCATGTTGCTCACGGAGG
GDF15	GGGTGTCGCTCCAGACCTATG	AGGAATCGGGTGTCTCAGGAAC
HAT1	GTGTAGAGGCAGATGATGTTGAG	CCTGTTGGACTGAGAACTGAG
α-Tublin	CCAGATGCCAAGTGACAAGAC	GTGCGAACTTCATCAATGACTG
GDF15-Promoter	AAGTGGTTTGTGTTCGTGAGTGC	TTCCTCACCGACAGCTTCCAT
PCR primer		
FOXA2-CDS	ATGCTGGGAGCGGTGAAGATG	TCAAGAGGAGTTCATAATGGGCCGGG
Foxa2-CDS	ATGCTGGGAGCCGTGAAGATG	CCCTTGTCCCCAGTGACCAGA
GDF15-CDS	ACAGCCATGCCCGGGCAAGAA	TTATATGCAGTGGCAGTCTTTGG
HAT1-CDS	ATGGCGGGATTTGGTGCTATGG	TTACAGATCCTCTTCAGAGATGAGTTT CTGCTCCAT
GDF15-Promoter_-2044 to -1079	CTTTCGAGGACAGTCACGAGCAT	ATCCTCTTGCCTCTGGCTCCC
GDF15-Promoter_-2044 to -1574	CTTTCGAGGACAGTCACGAGCAT	CACTCGCCTGGCTCTGCTTC
GDF15-Promoter_-2044 to -1779	CTTTCGAGGACAGTCACGAGCAT	GGTCAGGCCAGTCCGTCCAC
GDF15-Promoter_-1797 to +72	TGGACGGACTGGCCTGACCT	ACATCAGCAGCATCTGAGAGCATC
GDF15-Promoter_-1797 to -1574	TGGACGGACTGGCCTGACCT	CACTCGCCTGGCTCTGCTTC
GDF15-Promoter_-1594 to +72	GGAAGCAGAGCCAGGCGAGT	ACATCAGCAGCATCTGAGAGCATC
GDF15-Promoter_-1594 to -1079	GGAAGCAGAGCCAGGCGAGT	ATCCTCTTGCCTCTGGCTCCC
GDF15-Promoter_-1102 to +72	TTTGGGAGCCAGAGGCAAGAG	ACATCAGCAGCATCTGAGAGCATC

Supplemental Table 3. Key resources used in this study.

REAGENT or RESOURCE	SOURCE	IDENTIFIER
Antibodies		
Mouse anti-GAPDH (for WB 1:10000)	Cell Signaling Technology	Cat # 97166
Rabbit anti-FOXA2 (for WB 1:2000)	Abcam	Cat # ab108422
Rabbit anti-GDF15 (for WB 1:2000)	Proteintech	Cat # 27455-1-AP
Rabbit anti-HAT1 (for WB 1:1000, for IHC 1:500, and for IF 1:100)	Abcam	Cat # ab194296
Mouse anti-FOXA2 (for IHC 1:200, and for IF 1:100)	Santa Cruz	Cat # sc-101060
Rabbit anti-GDF15 (for IHC 1:50)	Abcam	Cat # ab206414
Rabbit anti-E-Cadherin (for WB 1:1000)	Cell Signaling Technology	Cat # 3195
Rabbit anti-N-Cadherin (for WB 1:1000)	Cell Signaling Technology	Cat # 13116
Rabbit anti-Slug (for WB 1:1000)	Cell Signaling Technology	Cat # 9585
Rabbit anti-pSTAT3-Y705 (for WB 1:10000)	Abcam	Cat # ab76315
Mouse anti-Pan-STAT3 (for WB 1:1000)	Santa Cruz	Cat # sc-8019
S-protein HRP Conjugate	Merck Millipore	Cat # 69047
HA Tag Polyclonal Antibody	Proteintech	Cat # 51064-2-AP
Myc-Tag (9B11) Mouse mAb	Cell Signaling Technology	Cat # 2276
S-protein Agarose	Merck Millipore	Cat # 69704
Anti-HA Magnetic Beads	Thermo Fisher Scientific	Cat # 88836
Anti-c-Myc Agarose	Thermo Fisher Scientific	Cat # 20168
Streptavidin Magnetic Beads	Thermo Fisher Scientific	Cat # 88816
Rabbit anti-H3K27ac (D5E4)	Cell Signaling Technology	Cat # 8173
Rabbit anti-H3K27me3 (C36B11)	Cell Signaling Technology	Cat # 9733
Rabbit anti-H3K4Me3 (C42D8)	Cell Signaling Technology	Cat # 9751
Rabbit anti-H3K4me (D1A9)	Cell Signaling Technology	Cat # 5326
Brilliant Violet 650™ anti-mouse CD45 (30-F11)	BioLegend	Cat # 103151
APC/Cyanine7 anti-mouse CD3 (17A2)	BioLegend	Cat # 100221
Brilliant Violet 421™ anti-mouse CD8a (53-6.7)	BioLegend	Cat # 100737
PE anti-mouse CD279 (PD-1, RMP1-30)	BioLegend	Cat # 109103
PE/Cyanine7 anti-mouse CD366 (Tim-3, RMT3-23)	BioLegend	Cat # 119716
APC anti-mouse CD197 (CCR7)	BioLegend	Cat # 120107
PE Rat IgG2b, κ Isotype Ctrl (RTK4530)	BioLegend	Cat # 400607
APC Rat IgG2a, κ Isotype Ctrl (RTK2758)	BioLegend	Cat # 400511
TruStain FcX™ PLUS (anti-mouse CD16/32, S17011E)	BioLegend	Cat # 156603
Rabbit anti-Tim3 (for mIHC 1:200)	Cell Signaling Technology	Cat # 83882
Rabbit anti-PD-1 (for mIHC 1:100)	Cell Signaling Technology	Cat # 84651
Rabbit anti-CD3 (for mIHC 1:100)	Abcam	Cat # ab16669
Rabbit anti-CD8α (for mIHC 1:100)	Cell Signaling Technology	Cat # 98941
Goat Anti Mouse IgG(H+L) (HRP)	Immunoway	Cat # RS0001
Goat Anti Rabbit IgG(H+L) (HRP)	Immunoway	Cat # RS0002

Goat anti-Rabbit IgG (H+L) Cross-Adsorbed Secondary Antibody, Alexa Fluor™ 488	Thermo Fisher Scientific	Cat # A-11008
Goat anti-Rabbit IgG (H+L) Cross-Adsorbed Secondary Antibody, Alexa Fluor™ 594	Thermo Fisher Scientific	Cat # A-11012
Normal mouse IgG	Santa Cruz	Cat # sc-2025
Chemicals, peptides, and recombinant proteins		
Zombie Red™ Fixable Viability Kit	BioLegend	Cat # 423109
TRIzol Reagent	Invitrogen	Cat # 15596018
Lipofectamine 3000 Transfection Reagent	Invitrogen	Cat # L3000015
RPMI 1640	Corning	Cat # 10-040-CV
DMEM	Gibco	Cat # C11995500BT
keratinocyte serum-free medium	Gibco	Cat # 17005-042
McCoy's 5A Medium	Gibco	Cat # 16600082
HyClone Fetal Bovine Serum	Gibco	Cat # 10099141C
D-Luciferin sodium salt	Abcam	Cat # ab145164
Recombinant Human GDF-15	R&D	Cat # 8146-GD
GDF15 ELISA Kit	Proteintech	Cat # KE00108
SimpleChIP® Plus Enzymatic Chromatin IP Kit	Cell Signaling Technology	Cat # 9005
Ponsegromab (PF 06946860)	MedChemExpress	Cat # HY-P99241
Pralsetinib (BLU-667)	MedChemExpress	Cat # HY-112301
C188-9 (TTI-101)	MedChemExpress	Cat # HY-112288
*InVivo*MAb anti-mouse PD-1 (CD279)	BioXCell	Cat # BE0146
Protease Inhibitor Cocktail	Cell Signaling Technology	Cat # 5872
Triton X-100	Sigma-Aldrich	Cat # 9036-19-5